Acta Pharmaceutica Sinica B 2022;12(10):3905–3923

Chinese Pharmaceutical Association
Institute of Materia Medica, Chinese Academy of Medical Sciences

Acta Pharmaceutica Sinica B

www.elsevier.com/locate/apsb
www.sciencedirect.com

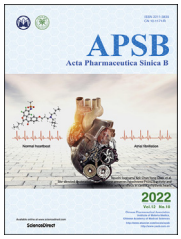

ORIGINAL ARTICLE

Site-directed deuteration of dronedarone preserves cytochrome P4502J2 activity and mitigates its cardiac adverse effects in canine arrhythmic hearts

Aneesh V. Karkhanis[a,†,‡], Gopalakrishnan Venkatesan[a,†,$], Ryuichi Kambayashi[b,†], Jacqueline Wen Hui Leow[a], Marcus Qingrui Han[a], Hiroko Izumi-Nakaseko[b], Ai Goto[b], Jeremy Kah Sheng Pang[c], Boon Seng Soh[c,d], Pipin Kojodjojo[e], Atsushi Sugiyama[b,*], Eric Chun Yong Chan[a,*]

[a]*Department of Pharmacy, Faculty of Science, National University of Singapore, Singapore 117543, Singapore*
[b]*Department of Pharmacology, Faculty of Medicine, Toho University, Tokyo 143-8540, Japan*
[c]*Institute of Molecular and Cell Biology, Agency for Science, Technology and Research, Singapore 138673, Singapore*
[d]*Department of Biological Sciences, Faculty of Science, National University of Singapore, Singapore 117558, Singapore*
[e]*Department of Medicine, Yong Loo Lin School of Medicine, National University of Singapore, Singapore 119228, Singapore*

Received 23 November 2021; received in revised form 13 January 2022; accepted 21 February 2022

KEY WORDS

Arachidonic acid;
Atrial fibrillation;

Abstract Cytochrome P4502J2 (CYP2J2) metabolizes arachidonic acid (AA) to cardioprotective epoxyeicosatrienoic acids (EETs). Dronedarone, an antiarrhythmic drug prescribed for treatment of atrial fibrillation (AF) induces cardiac adverse effects (AEs) with poorly understood mechanisms.

*Corresponding authors. Tel.: +81 3 37624151 (ext 2361), fax: +81 3 54935413 (Atsushi Sugiyama); Tel.: +65 65166137, fax: +65 67791554 (Eric Chun Yong Chan).

E-mail addresses: atsushi.sugiyama@med.toho-u.ac.jp (Atsushi Sugiyama), phaccye@nus.edu.sg (Eric Chun Yong Chan).

†These authors made equal contributions to this work.

‡ *Current: A*STAR Skin Research Labs, Agency for Science, Technology and Research, Singapore 138665, Singapore*

$ *Current: Antimicrobial Resistance Interdisciplinary Research Group, Singapore-MIT Alliance for Research and Technology, Singapore 138602, Singapore*

Peer review under responsibility of Chinese Pharmaceutical Association and Institute of Materia Medica, Chinese Academy of Medical Sciences.

https://doi.org/10.1016/j.apsb.2022.03.008

CYP2J2;
Drug-induced proarrhythmia;
Epoxyeicosatrienoic acids;
Mechanism-based inactivation;
Dronedarone

We previously demonstrated that dronedarone inactivates CYP2J2 potently and irreversibly, disrupts AA-EET pathway leading to cardiac mitochondrial toxicity rescuable *via* EET enrichment. In this study, we investigated if mitigation of CYP2J2 inhibition prevents dronedarone-induced cardiac AEs. We first synthesized a deuterated analogue of dronedarone (termed poyendarone) and demonstrated that it neither inactivates CYP2J2, disrupts AA-EETs metabolism nor causes cardiac mitochondrial toxicity *in vitro*. Our patch-clamp experiments demonstrated that pharmacoelectrophysiology of dronedarone is unaffected by deuteration. Next, we show that dronedarone treatment or CYP2J2 knockdown in spontaneously beating cardiomyocytes indicative of depleted CYP2J2 activity exacerbates beat-to-beat (BTB) variability reflective of proarrhythmic phenotype. In contrast, poyendarone treatment yields significantly lower BTB variability compared to dronedarone in cardiomyocytes indicative of preserved CYP2J2 activity. Importantly, poyendarone and dronedarone display similar antiarrhythmic properties in the canine model of persistent AF, while poyendarone substantially reduces beat-to-beat variability of repolarization duration suggestive of diminished proarrhythmic risk. Our findings prove that deuteration of dronedarone prevents CYP2J2 inactivation and mitigates dronedarone-induced cardiac AEs.

1. Introduction

Omega-6 polyunsaturated fatty acids such as arachidonic acid (AA) undergo cytochrome P450 (CYP)-dependent metabolism to epoxides that play important roles in cardiac pathophysiology[1]. CYP2J2, an abundant cardiac epoxygenase[2,3] metabolizes AA to four regioisomeric epoxyeicosatrienoic acids (EETs, Supporting Information Fig. S1)[4]. EETs are lipid mediators with vasodilatory, angiogenic, anti-apoptotic, anti-inflammatory and ion channel regulatory functions[5]. EETs are further deactivated to less potent dihydroxyeicosatrienoic acids by soluble epoxide hydrolase (Fig. S1)[6]. Owing to cardioprotective roles of EETs, transgenic mice with cardiac-specific overexpression of CYP2J2 were developed[7]. These mice exhibited a higher rate of EET biosynthesis and hence were protected from several cardiac pathologies including doxorubicin-induced cardiotoxicity, ventricular tachyarrhythmia and atrial arrhythmogenicity[8−10]. Conversely, perturbations in cardiac CYP2J2 expression and EET biosynthesis initiate and progress maladaptive cardiac hypertrophy[11,12]. Despite the increasing knowledge of CYP2J2 functions, its role in drug-induced cardiac adverse effects (AEs) and specifically proarrhythmic risk remains unknown.

CYP2J2 metabolizes not only endobiotics such as AA but also several xenobiotics and is inhibited byamiodarone, astemizole, dronedarone and terfenadine[13−15]. Amiodarone (Fig. 1A) and dronedarone (Fig. 1A) are multiple ion channel blocking Class III antiarrhythmic drugs. Amiodarone is highly efficacious in maintaining sinus rhythm in atrial fibrillation (AF) patients but is associated with severe lung and thyroid toxicities[16] partly due to its extensive tissue accumulation[17]. Dronedarone, a non-iodinated analogue of amiodarone, has less extensive tissue accumulation and organ toxicities[18] due to favorable pharmacokinetics. Dronedarone is prescribed in paroxysmal and persistent AF[19] yet it is contraindicated in patients with permanent AF or decompensated heart failure due to increased mortality[20,21]. Beyond exacerbation of heart failure, dronedarone was reported to precipitate pathological ventricular proarrhythmia and Torsades de Pointes (TdP) in cardio-hemodynamically compromised patients[22,23]. We previously reported that dronedarone inactivates CYP2J2 irreversibly and perturbs the AA-EETs metabolic axis[13,24,25]. Taken together, we postulate that the inactivation of CYP2J2 and the subsequent perturbation of AA-EET metabolism contributes towards drug-induced cardiac AEs and particularly drug-induced proarrhythmia.

In previous work, we proved that dronedarone undergoes CYP2J2-mediated desulphonation followed by formation of hydroxylamino-aryl metabolite and finally quinone oxime reactive intermediate, which in turn inactivates CYP2J2[13]. In other words, the benzofuran ring on dronedarone is metabolically susceptible to reactive intermediate formation. Hence, it became important in this study to design a probe molecule that is devoid of CYP2J2 inhibition property yet preserves the multiple ion channel inhibitory pharmacology of dronedarone to investigate the role of CYP2J2 in drug-induced proarrhythmia. Specifically, we attempted to reduce CYP2J2-mediated bioactivation of dronedarone *via* a site-directed deuterated analogue, herein termed as poyendarone (Fig. 1A). Deuteration is a chemical process where at least one hydrogen atom in the molecule is substituted by deuterium. Since deuterium has greater atomic mass, carbon−deuterium (C−D) bond cleavage energy is relatively higher (341.4 kJ/mol) than that of carbon−hydrogen (C−H) bond (338.4 kJ/mol)[26]. This difference in bond dissociation energy is due to the lower vibrational energy and lower zero-point energy of C−D vis-à-vis C−H bond[27]. As it is relatively difficult to break C−D bond, deuteration is an excellent strategy to prevent proton loss on metabolically labile chemical groups and prevent reactive metabolite formation.

Here, we report that poyendarone exhibits comparable physicochemical, metabolic, and cardiac ion channel inhibitory properties as dronedarone but neither inactivates CYP2J2, disrupts AA-EET metabolism, causes mitochondrial toxicity nor increases beat-to-beat (BTB) variability in cardiomyocytes. By preserving CYP2J2 metabolic function and multiple ion channel inhibitory pharmacology, poyendarone demonstrates comparable efficacy in a persistent AF canine model while it substantially reduces beat-

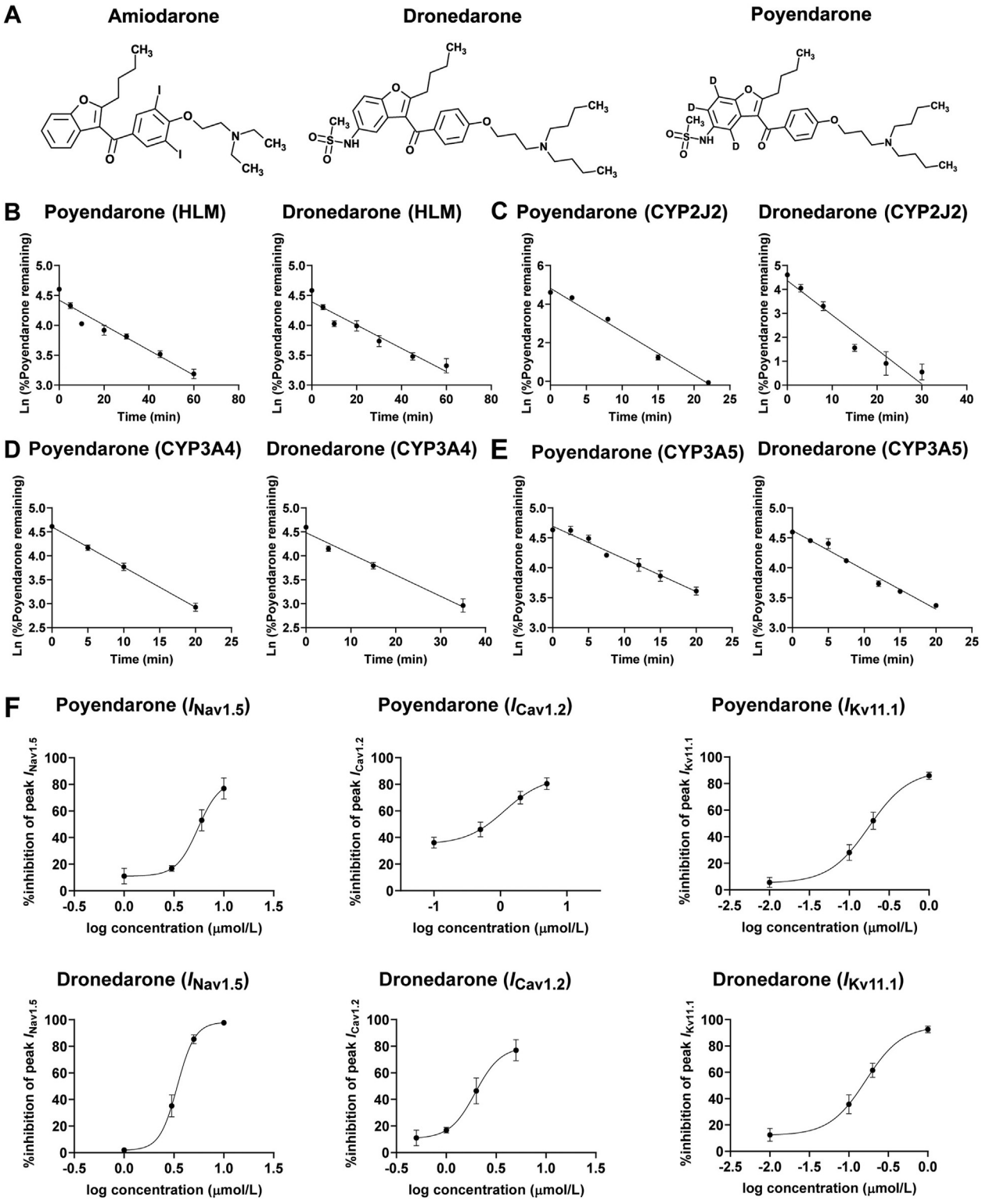

Figure 1 Deuteration of dronedarone preserves its metabolic and pharmacological activities but mitigates the inactivation of CYP2J2. Chemical structures of (A) amiodarone (left), dronedarone (middle) and poyendarone (right). Poyendarone is structurally identical to dronedarone except for the replacement of hydrogen atoms with deuterium, D on positions 4, 5,7 on benzofuran ring. (B) HLM metabolizes poyendarone (left) and dronedarone (right) to the same extent *via* the first-order kinetics indicated by linear decline in the logarithm of percentage drug remaining (*y*-axis) with increasing incubation time (*x*-axis). Similarly, (C) CYP2J2, (D) CYP3A4 and (E) CYP3A5 metabolizes poyendarone (left) and dronedarone (right) to the same extent *via* the first-order kinetics. (F) *In vitro* blockade of $Na_V1.5$ (left), $Ca_V1.2$ (middle) and $K_V11.1$ (right) currents by poyendarone (upper panel) or dronedarone (lower panel). The dose−response curve represents percentage blockade of each current against logarithm of concentration. The graphs were plotted using GraphPad Prism software v8.4.2 (San Diego, CA, USA).

to-beat variability of repolarization duration (BVR) indicative of diminished proarrhythmic risk as compared to dronedarone.

2. Results

2.1. Poyendarone and dronedarone have similar physicochemical, metabolic, and electrophysiological properties

The *c*log*P* values for both compounds were 7.2 (Table 1). The aqueous solubility of poyendarone (2.43 ± 0.25 μg/mL) was comparable to dronedarone (3.22 ± 0.34 μg/mL, $P > 0.05$). Similarly, the effective permeability yielded a non-significant difference between poyendarone ($4.08 \pm 0.5 \times 10^{-6}$ cm/s) and dronedarone ($3.46 \pm 0.5 \times 10^{-6}$ cm/s, $P > 0.05$). Thus, site-directed deuteration of dronedarone preserved the key physicochemical properties.

Intrinsic clearance (CL_{int}) is a key parameter to evaluate the hepatic and extrahepatic clearance of drugs. CL_{int} of poyendarone and dronedarone were measured in human liver microsomes (HLM), CYP2J2, CYP3A4 and CYP3A5. HLM is physiologically relevant hepatic enzyme system, CYP2J2 is an abundant cardiac enzyme while CYP3A4 and CYP3A5 are major drug metabolizing enzymes. The percentages of poyendarone and dronedarone remaining in HLM (Fig. 1B), CYP2J2 (Fig. 1C), CYP3A4 (Fig. 1D) and CYP3A5 (Fig. 1E) decreased monoexponentially with increasing incubation time, establishing the first-order elimination kinetics essential for determining CL_{int}. The metabolic half-life ($t_{1/2}$), elimination rate constant (k) and CL_{int} values of poyendarone and dronedarone were comparable across all four enzyme systems (Table 1) confirming that deuteration did not modify the hepatic and extrahepatic clearance of dronedarone.

Since dronedarone is a multiple cardiac ion channel blocker[28], we investigated if poyendarone exhibited similar electrophysiological properties *in vitro*. HEK293FT cells were co-transfected with $hNa_V1.5$, $hCa_V1.2$ or $hK_V11.1$ (commonly known as human ether-a-go-go-related gene (hERG)) channel plasmids and their respective auxiliary subunits. These cells were subjected to whole-cell patch-clamp recording and the currents namely I_{Na}, L-type Ca^{2+} ($I_{Ca,L}$), and rapid delayed rectifier K^+ (I_{Kr}) respectively were measured. We tested blockade of specific subunits of cardiac ion channels namely $Na_V1.5$, $Ca_V1.2$, $K_V11.1$ due to their significance in initiation and propagation of cardiac action potential. Both dronedarone and poyendarone caused concentration-dependent blockade of $Na_V1.5$ peak current (Fig. 1F, Supporting Information Fig. S3), $Ca_V1.2$ peak current (Fig. 1F, and Supporting Information Fig. S4) and $K_V11.1$ tail current (Fig. 1F, and Supporting Information Fig. S5). Dose-response curves indicate comparable IC_{50} values against these currents for poyendarone and dronedarone (Table 1). In summary, deuteration of dronedarone neither alters its physicochemical properties, hepatic and extrahepatic clearance nor multiple ion channel inhibitory pharmacology.

2.2. Poyendarone demonstrates diminished mechanism-based inactivation (MBI) of CYP2J2

The pre-incubation time-dependency and concentration-dependency of MBI is confirmed when CYP2J2 activity decreases with increasing pre-incubation time of inactivator in the absence of a probe substrate and concentration of inactivator respectively. The concentration-dependency of MBI is also evident in the saturation kinetics where observed rate constants of inactivation (k_{obs}) approach maximum plateau as inactivator concentration increases. Using rivaroxaban as a specific probe substrate of CYP2J2, poyendarone was determined not to cause MBI of CYP2J2 while dronedarone potently inactivated CYP2J2-mediated rivaroxaban hydroxylation (Fig. 2A, and Table 2). Using astemizole as another specific probe substrate of CYP2J2, poyendarone similarly yielded 62-fold less potent MBI of CYP2J2-mediated astemizole *O*-desmethylation ($k_{inact}/K_I = 0.008$ L/μmol·min) as compared to dronedarone ($k_{inact}/K_I = 0.5$ L/μmol·min, Supporting Information Figs. S6A–D). These observations confirmed the lower extent of bioactivation of poyendarone to the quinone-oxime intermediate and corroborated the kinetically slower abstraction of deuterium from a C–D bond[29]. Furthermore, substrate-dependent effect on MBI potencies of dronedarone and poyendarone was observed which could be explained by CYP2J2 inhibitory effect of astemizole but not rivaroxaban. Substrates such as astemizole,

Table 1 Physicochemical, metabolic, and electrophysiological properties of dronedarone and poyendarone.

Property		Poyendarone	Dronedarone
Physicochemical properties			
*c*Log*P*		7.2	7.2
Aqueous solubility (μg/mL) (24 h, pH 7.4)		2.43 ± 0.25	3.22 ± 0.34
Effective permeability (cm/s) (pH 7.4)		$4.08 \pm 0.5 \times 10^{-6}$	$3.46 \pm 0.5 \times 10^{-6}$
Metabolic stability			
Metabolic half-life ($t_{1/2}$) min	CYP2J2	5.32	3.95
	CYP3A4	7.80	8.05
	CYP3A5	17.78	12.21
	HLM	10.26	10.45
Intrinsic clearance, CL_{int} (μL/min/pmol)	CYP2J2	0.65	0.88
	CYP3A4	0.89	0.86
	CYP3A5	0.39	0.57
Intrinsic clearance, CL_{int} (μL/min/mg)	HLM	13.51	13.26
Ion channel blocking activity			
$Na_v1.5$ peak current blockade IC_{50} (μmol/L)		5.51	3.41
$Ca_v1.2$ peak current blockade IC_{50} (μmol/L)		1.15	1.96
$K_V11.1$ tail current blockade IC_{50} (μmol/L)		0.17	0.16

HLM: Human liver microsomes

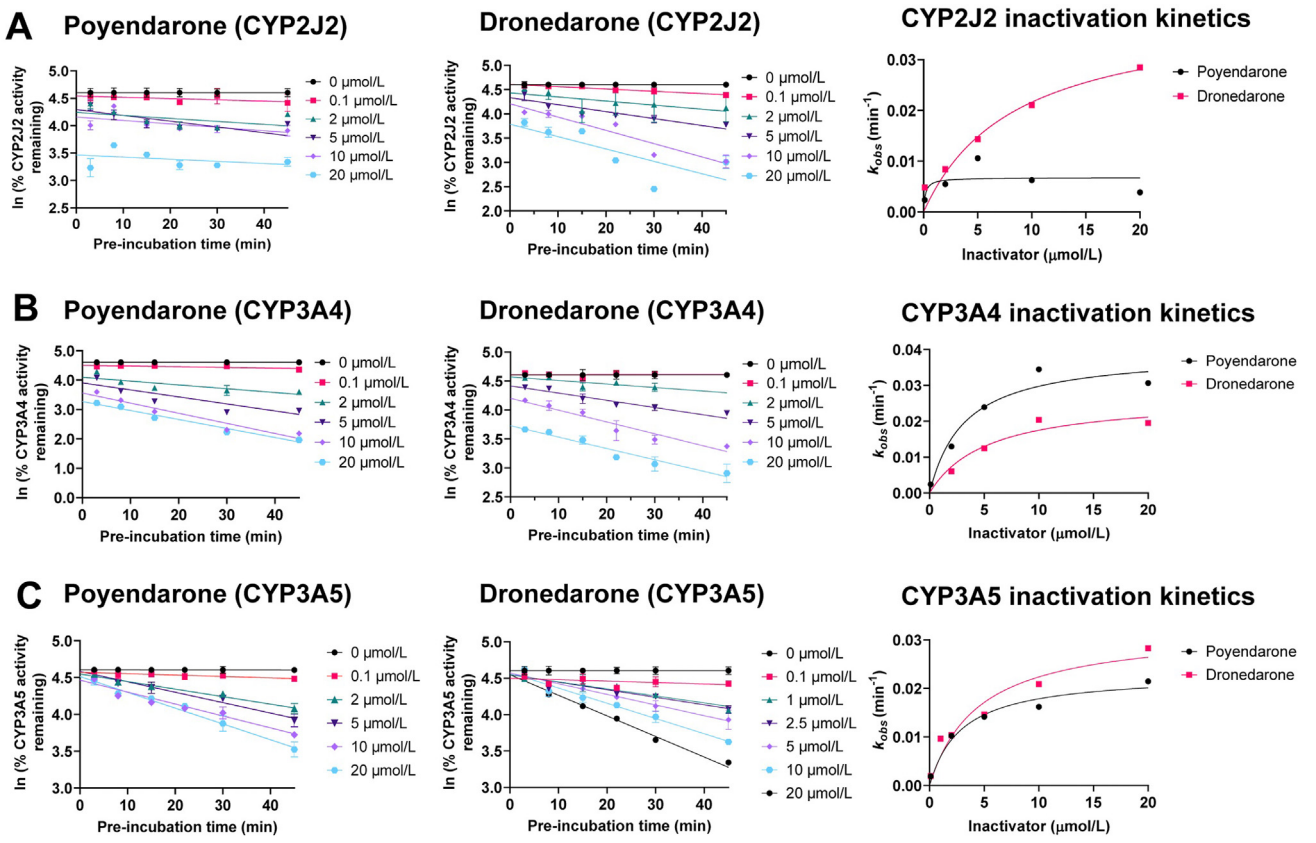

Figure 2 Time-, concentration-dependent inactivation of CYP2J2, CYP3A4 and CYP3A5 activity by poyendarone and dronedarone with rivaroxaban as probe substrate. The logarithm of percentage (A) CYP2J2, (B) CYP3A4 and (C) CYP3A5 activity was plotted against pre-incubation time in the presence of poyendarone (left) and dronedarone (middle) with rivaroxaban as substrate. The observed inactivation rate (k_{obs}) for CYP2J2, CYP3A4 or CYP2A5 was plotted against the inactivator concentration (right) to calculate k_{inact} and K_I for poyendarone and dronedarone (Table 2). Each point represents mean ± SEM of three experiments. The graphs were plotted using GraphPad Prism software v8.4.2 (San Diego, CA, USA).

terfenadine, ebastine, and AA exhibit substrate-dependent auto-inhibition of CYP2J2 which are expected to overestimate the inhibitory potency of a test inhibitor such as poyendarone[30–34]. In contrast, more accurate MBI kinetics were characterized using rivaroxaban as probe substrate as it does not exhibit autoinhibition of CYP2J2.

We employed L-glutathione (GSH) trapping assay to ascertain the nature of reactive intermediates. GSH is a common nucleophilic agent used to trap soft electrophiles such as reactive metabolites. Experimentally, reactions with CYP2J2, test drugs, NADPH generating system and GSH were incubated, quenched and the supernatant was concentrated to analyze the GSH-reactive metabolite adducts using LC−MS/MS. The precursor ion at mass to charge ratio (m/z) 802 and 800 indicated detection of GSH conjugates of poyendarone (Supporting Information Fig. S7A) and dronedarone (Supporting Information Fig. S7B), respectively. But quinone-oxime nature of the reactive intermediates was confirmed based on key product ions with m/z = 481 or m/z = 479 for poyendarone or dronedarone, respectively. The mass spectra associated with the quinone-oxime-GSH conjugates of poyendarone and dronedarone confirmed the electrophilicity of their respective intermediates in reacting with

Table 2 CYP2J2, CYP3A4 and CYP3A5 inactivation kinetic parameters for poyendarone and dronedarone using rivaroxaban as a substrate. K_I and k_{inact} are represented as mean ± SEM.

CYP450 enzyme	Inactivator	k_{inact} (min^{-1})	K_I (μmol/L)	k_{inact}/K_I (L/mol·min)
CYP2J2	Poyendarone	n.d.	n.d.	n.d.
	Dronedarone	0.0400 ± 0.008	8.47 ± 3.96	0.00471
CYP3A4	Poyendarone	0.0392 ± 0.0055	3.19 ± 1.52	0.0123
	Dronedarone	0.0267 ± 0.0054	5.3 ± 2.95	0.00505
CYP3A5	Poyendarone	0.0231 ± 0.0022	2.91 ± 0.97	0.00793
	Dronedarone	0.0323 ± 0.0045	4.44 ± 1.76	0.00728

n.d.: not determined as poyendarone does not inactivate CYP2J2.

nucleophiles such as GSH. However, it must be emphasized that the relative abundance of quinone-oxime-GSH conjugates of poyendarone was about 6-fold lower than that of dronedarone corroborating the reduced MBI of CYP2J2 by poyendarone.

It is known that dronedarone also exhibits potent MBI of CYP3A4 and CYP3A5[35]. Since we aimed to design a chemical probe that preserves the biological activities of dronedarone but only mitigates its CYP2J2 inactivation, we investigated if deuteration of dronedarone would attenuate its inactivation of additional CYP3A isoforms. Using rivaroxaban as a probe substrate, dronedarone and poyendarone inactivated CYP3A4 (Fig. 2B) and CYP3A5 (Fig. 2C) in a preincubation time-dependent and concentration-dependent manner. Poyendarone demonstrated 2.4-fold higher inactivation potency (k_{inact}/K_I = 0.0123 L/μmol·min) than dronedarone (k_{inact}/K_I = 0.0050 L/μmol·min) for CYP3A4 while comparable potencies for CYP3A5 inactivation were observed for poyendarone and dronedarone (k_{inact}/K_I = 0.0063 L/μmol·min, vis-à-vis k_{inact}/K_I = 0.0079 L/μmol·min, Table 2). In conclusion, site-directed deuteration of dronedarone abrogated its potent MBI of CYP2J2 while its inactivation of CYP3A4 and CYP3A5 was marginally affected.

2.3. *Poyendarone preserves CYP2J2-mediated AA metabolic activity*

Previously, we determined that dronedarone potently inhibits CYP2J2-mediated AA metabolism to EETs[25]. We performed the same assay with poyendarone and dronedarone concurrently and demonstrated that poyendarone did not yield concentration-dependent inhibition of CYP2J2-AA metabolism (Fig. 3). In other words, poyendarone prevents CYP2J2 inhibition and preserves *in situ* EET levels.

2.4. *Poyendarone reduces mitochondrial toxicity in cardiomyocytes*

Previously, we have shown that dronedarone causes significant mitochondrial toxicity in rat cardiac H9c2 cells by dissipating mitochondrial membrane potential, inhibiting complex I & II of the electron transport chain (ETC), uncoupling of ETC, reducing intracellular ATP and thus leading to cell death in a concentration-dependent manner[24]. Notably, these dronedarone-induced cardiac mitochondrial dysfunctions were mitigated by pre-treatments with 11,12-EET and 14,15-EET, underpinning the indirect dysregulation of the AA-EETs metabolic axis[24]. Hence, we investigated if poyendarone that is devoid of CYP2J2 inactivation would reduce mitotoxic effects on cardiomyocytes. After exposure of H9c2 cells to poyendarone and dronedarone for 6 h, the dead cell-related protease fluorescence signal increased in a concentration-dependent manner, confirming the 22-fold higher cytotoxicity of dronedarone (EC_{50} = 1.21 ± 1.7.23 μmol/L) than poyendarone (EC_{50} = 27.63 ± 2.34 μmol/L, Fig. 4A). Simultaneously, dronedarone decreased intracellular ATP levels (IC_{50} = 3.10 ± 1.46 μmol/L) 13-fold more potently than poyendarone (IC_{50} = 41.52 ± 1.29 μmol/L, Fig. 4A).

To investigate the mechanism of ATP reduction, we measured the inhibition of oxygen consumption rate (OCR) by

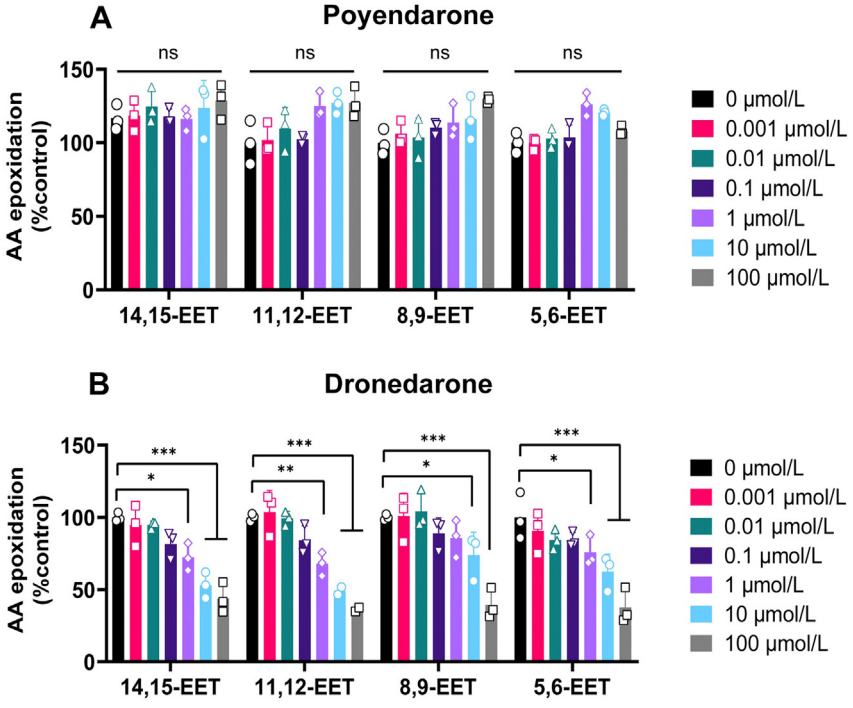

Figure 3 Percentage of AA metabolized to each respective EET (*y*-axis) by CYP2J2 was plotted against increasing concentration of (A) poyendarone or (B) dronedarone (*x*-axis). Dronedarone inhibits CYP2J2-mediated AA metabolism in a concentration-dependent manner. Poyendarone prevents CYP2J2-mediated inhibition of AA metabolism and maintains EET levels at highest tested concentration. Each bar represents mean ± SEM of one experiment performed in triplicates. The different groups were compared with two-way ANOVA followed by Tukey's *post-hoc* correction and statistical significance was determined when $^{*}P < 0.05$, $^{**}P < 0.01$, $^{***}P < 0.001$, $^{\#}P < 0.0001$. Analysis was performed using GraphPad Prism software v8.4.2 (San Diego, CA, USA).

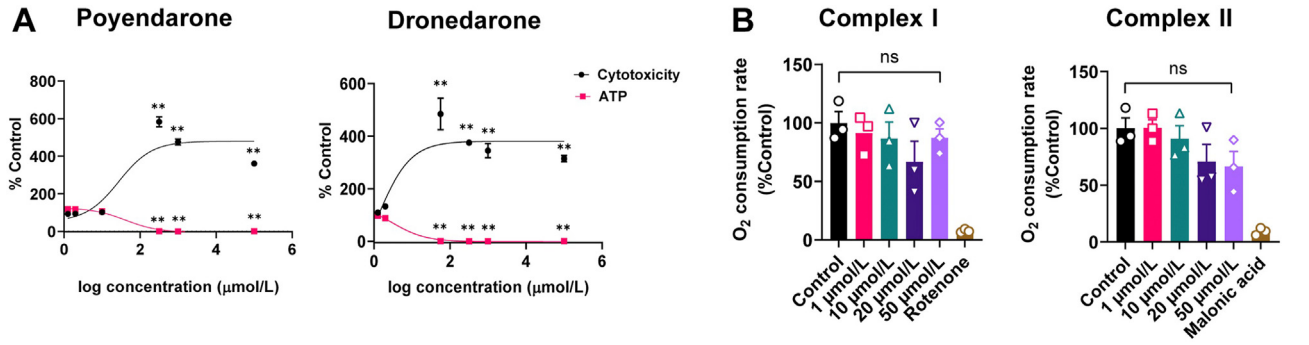

Figure 4 Poyendarone exhibits lower mitochondrial toxicity in isolated mitochondria. (A) Mitochondrial toxicity profiles in H9c2 cells incubated with increasing concentrations of poyendarone. Both cytotoxicity (black) and ATP levels (magenta) are expressed as percentages of control. Data represented as the mean ± SEM of experiments performed across three cell passages in triplicates. Increasing concentrations of poyendarone and dronedarone were compared with control (0 μmol/L) with one-way ANOVA followed by Dunnett's *post-hoc* correction. (B) Lack of inhibition of NADH- or succinate-supplemented ETC activity by poyendarone in isolated rat heart mitochondria. Rotenone (2 μmol/L) or malonic acid (1 mmol/L) was positive inhibitor for complex I and II, respectively. The graph represents the OCR (as % control), reflective of the activity of the mitochondrial complexes I and II inhibitor concentrations. Each bar shows mean ± SEM for three mitochondrial preparations. Different groups were compared with control with one-way ANOVA followed by Dunnett's *post-hoc* correction. Statistical significance was confirmed when $^{**}P < 0.01$ two-way. Analysis was performed using GraphPad Prism software v8.4.2 (San Diego, CA, USA).

poyendarone against complex I & II of the mitochondrial ETC in isolated rat heart mitochondria. Poyendarone lacked inhibition of NADH-dependent (IC_{50} = 80.42 μmol/L) and succinate-dependent (IC_{50} = 66.70 μmol/L) ETC activities at physiological concentrations (Fig. 4B). Compared to previously reported data on dronedarone[24], poyendarone yielded 26-fold and 5-fold lower potency in inhibiting complex I and II, respectively. In summary, site-directed deuteration of dronedarone reduced its mitochondrial toxicity in cardiomyocytes by abrogating ATP depletion and inhibition of ETC complex I & II.

2.5. *Chemical and gene knockdown of CYP2J2 increases BTB variability in human induced pluripotent stem cell-derived cardiomyocytes (hiPSC-CMs)*

Our *in vitro* patch-clamp data demonstrated that dronedarone and poyendarone block multiple ion channels with comparable potencies. Additionally, dronedarone potently inactivates CYP2J2 while poyendarone lacks a similar action. Consequently, poyendarone is a suitable chemical probe to investigate the role of CYP2J2 metabolism in drug-induced proarrhythmia. Here, we first established that CYP2J2 is abundantly expressed in untreated spontaneously beating hiPSC-CMs clusters (Fig. 5A). Dronedarone, but not poyendarone and amiodarone, inhibited CYP2J2-mediated astemizole *O*-desmethylation by 98% ($P < 0.05$) at physiological drug concentration levels in hiPSC-CM (Fig. 5B, Supporting Information Fig. S8A).

Several research groups have utilized hiPSC-CM to predict *in vitro* drug-induced proarrhythmia using BTB variability derived from Poincaré plots[36,37]. In dronedarone-treated hiPSC-CM, the BTB variability increased with drug concentrations indicated by high scattering and incoherence compared to poyendarone or amiodarone based on visual inspection (Fig. 5C, Fig. S8B). Quantitatively, dronedarone induced 4-fold ($P < 0.05$) and 3-fold ($P < 0.05$) short-term variability (STV_{RR}) and long-term variability (LTV_{RR}) respectively compared to poyendarone at 1 μmol/L concentration (Fig. 5D and E, Fig. S8C). In conclusion, dronedarone markedly inhibited CYP2J2 activity and induced significantly higher BTB variability as compared to poyendarone at physiologically relevant concentrations in hiPSC-CM.

Next, we questioned if CYP2J2 gene knockdown would contribute directly towards proarrhythmic effect. Here, CYP2J2 knockdown in hiPSC-CM was first performed using four different siRNAs (Supporting Information Table S1). Subsequently, calcium transient currents reflective of single cardiac contractions were measured. All siRNAs diminished CYP2J2 expression by 40%−80% with siRNA-1 and siRNA-3 being the most effective (Fig. 6A). Using siRNA knockdown, calcium transient durations (CTD) were computed from the start of calcium depolarization to the 90% repolarization mark in each cardiac contraction, and the mean across all contractions was computed per cluster. The BTB interval and variation between beats (BTB variability) were further computed between two cardiac contractions per cluster of hiPSC-CM. CYP2J2 knockdown cells exhibited significantly higher mean CTD (Fig. 6B), mean BTB interval (Fig. 6C) and BTB variability (Fig. 6D, Table 3). Poincaré plots revealed significant BTB variability for CYP2J2 knockdown hiPSC-CM clusters (Fig. 6E, right panel) as compared to control (Fig. 6E, left panel). Quantitatively, the knockdown of CYP2J2 in hiPSC-CM resulted in 1.7-fold ($P < 0.05$) and 1.6-fold ($P < 0.05$) greater STV_{RR} (Fig. 6F) and LTV_{RR} respectively, as compared to control (Fig. 6, and Table 3). The results of individual siRNAs for all measured endpoints were broadly consistent (Fig. S9A−F, Supporting Information Table S2). In summary, both chemical inhibition and gene knockdown of CYP2J2 result in a consistent increase in BTB variability as observed in spontaneously beating human cardiomyocytes.

2.6. *Poyendarone preserves anti-atrial fibrillatory effects in canine model of persistent AF*

Early evidence from *in vitro* patch-clamp and BTB variability experiments signaled a favorable antiarrhythmic and reduced proarrhythmic risk of poyendarone. To confirm these effects *in vivo*, poyendarone and dronedarone were studied previously in healthy dogs[38,39] and in canine model of paroxysmal AF induced by chronic atrioventricular block[40]. Poyendarone showed atrial selectivity and lacked ventricular proarrhythmic propensity in both studies. In this study, persistent AF was induced by atrial tachypacing for >6 weeks to the atria of

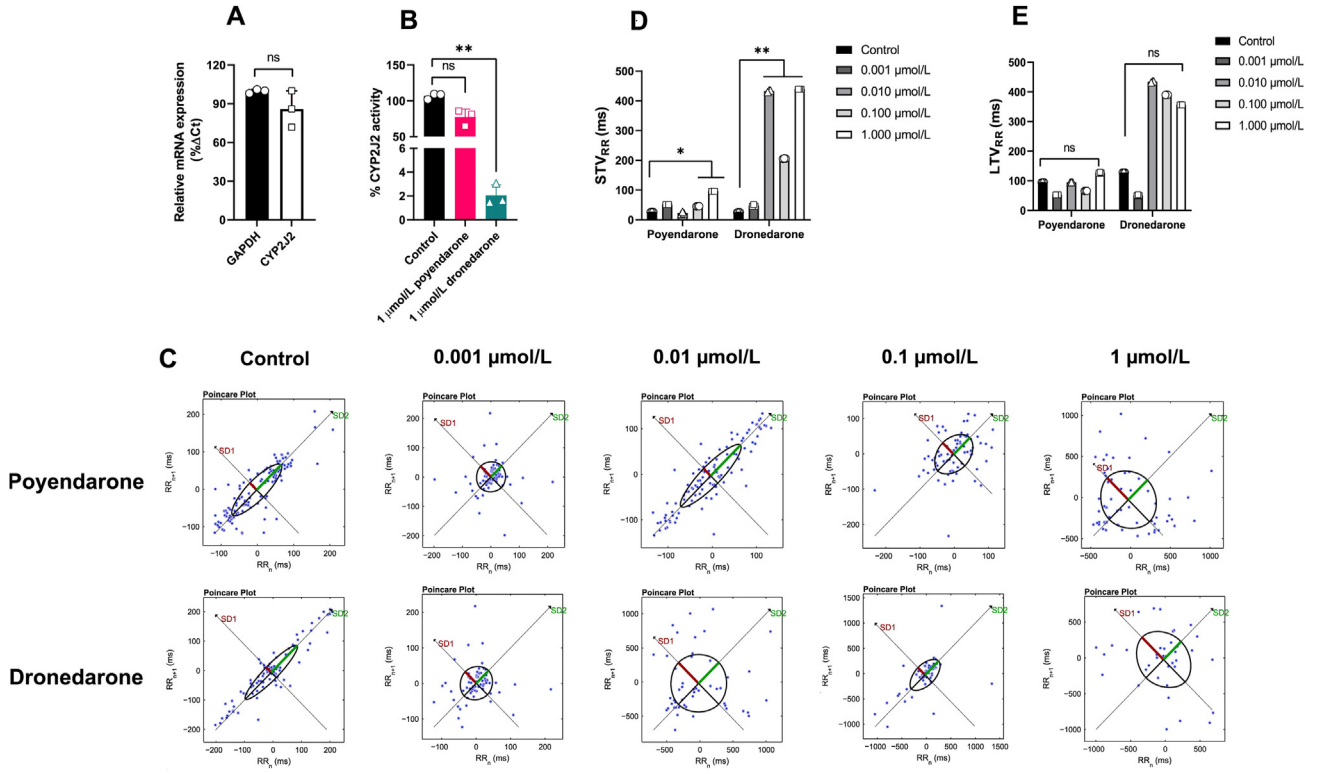

Figure 5 Dronedarone but not poyendarone inhibits CYP2J2 and causes BTB variability at physiological concentration. (A) The percentage of CYP2J2 gene expression in hiPSC-CMs relative to GAPDH. (B) Inhibition of CYP2J2 in hiPSC-CMs. Percentage CYP2J2 activity was plotted against 1 μmol/L poyendarone or dronedarone. Each bar represents mean ± SEM of three experiments performed in triplicates. The groups were compared with one-way ANOVA followed by Dunnett's *post-hoc* correction. (C) The Poincaré plots of control, 0.001−1 μmol/L poyendarone (upper panel) and dronedarone (lower panel). Points encompassed in an ellipse and aligned to line of identity indicate minimum BTB variability while scattered points indicate high BTB variability. (D) SD1 or STV_{RR} and (E) SD2 or LTV_{RR} of control, 0.001−1 μmol/L dronedarone and poyendarone. Each bar represents mean ± SEM of one experiment performed in triplicates. Different groups were compared with control with one-way ANOVA followed by Dunnett's *post-hoc* correction. Statistical significance was confirmed when $^{*}P < 0.05$, $^{**}P < 0.01$, $^{***}P < 0.001$, $^{\#}P < 0.0001$. Analysis was performed using GraphPad Prism software v8.4.2 (San Diego, CA, USA).

chronic atrioventricular block dogs and the anti-AF activity of the drugs was measured (Fig. 7A)[41]. No animals exerted any lethal ventricular arrhythmia or hemodynamic collapse leading to their death during the experimental period. Animals were constantly monitored with Holter electrocardiogram for 21 h. Poyendarone terminated the persistent AF in 2 out of 4 animals at 12.3 h (#1) and 6.1 h (#3) after the start of the administration, whereas dronedarone terminated the AF in 2 out of 4 animals at 5.2 h (#1) and 10.6 h (#4) (Fig. 7B). Amiodarone, as a control drug, converted the AF into sinus rhythm at 7.7 h (#1) and 5.9 h (#3) after the start of administration; thereafter, the AF spontaneously recurred in the former at 5.2 h (#1) after the termination of AF (Supporting Information Figs. S10A and B). Vehicle control (ethanol) did not terminate the AF in any animal during 21 h observation period after its administration (Fig. S10).

2.7. *Poyendarone displays lower BVR in canine model of persistent AF*

To assess the drug-induced proarrhythmic risk *in vivo*, we measured corrected QT interval (QTcF) and short-term variability of ventricular repolarization (STV_{QT}). The four parameters namely, QTcF, change in QTcF from its basal control at each time point (ΔQTcF), STV_{QT} and change in STV_{QT} from its basal control at each time point (ΔSTV_{QT}) after the administration of drugs are summarized in Fig. 7C. The pre-drug basal control values of the QTcF and STV_{QT} (ms) were 267 ± 14 and 2.82 ± 0.32 in poyendarone-, 261 ± 17 and 2.82 ± 0.13 in dronedarone-, 236 ± 18 and 2.25 ± 0.14 in amiodarone-, and 261 ± 9 and 2.41 ± 0.14 in ethanol-treated animals ($n = 4$ for each group), respectively. No significant difference was observed in these pre-drug basal control values among the groups. Poyendarone, dronedarone, and amiodarone tended to prolong the QTcF with peak changes of +7 ± 5, +16 ± 11 and +6 ± 7 at 0.5 h after their administrations, respectively, which did not achieve statistical significance (Fig. 7C, and Figs. S10C and D). In addition, poyendarone and ethanol shortened the QTcF at 6 h after their infusion. Meanwhile, dronedarone increased the STV_{QT} for 0.5−12 h after its administration, of which peak increment was 3.06 ± 0.80 ms at 3 h. Poyendarone and amiodarone tended to increase the STV_{QT}, of which increments were 1.21 ± 0.49 ms at 9 h and 1.05 ± 0.41 ms at 1 h, respectively, which did not achieve statistical significance (Fig. 7C, and Fig. S10E and F). Most importantly, poyendarone did not elevate STV_{QT} >5 ms while dronedarone intermittently elevated STV_{QT} throughout the observation period. Since STV_{QT} >5 ms is a critical border for the onset of early afterdepolarization, our

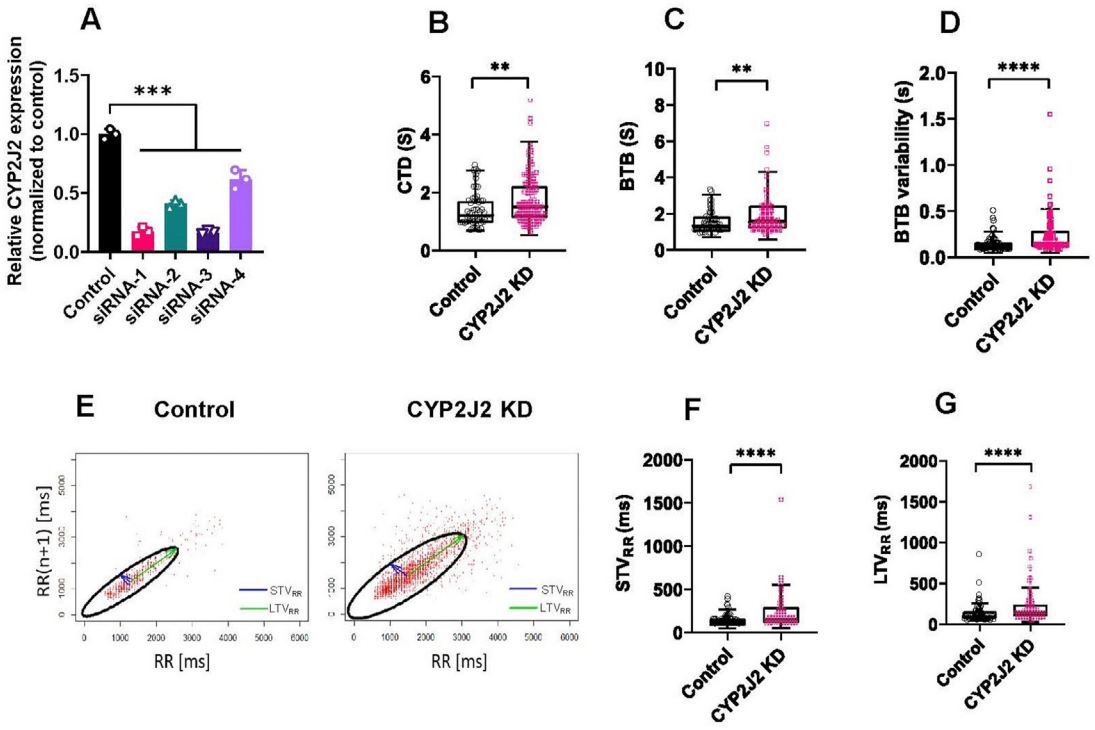

Figure 6 CYP2J2 knockdown (CYP2J2 KD) perturbed electrophysiological properties in cardiac cells. (A) qPCR was performed 96 h post-siRNA transfection where there was a 40%−80% knockdown of *CYP2J2* compared to the control treatment across all siRNA treatments. Comparison were performed with one-way ANOVA followed by Dunnett's *post hoc* test (***$P < 0.001$, $n = 3$). CYP2J2 KD exhibited higher (B) mean calcium transient duration (CTD), (C) mean beat-to-beat (BTB) interval and (D) BTB variability. (E) Poincaré plots were mapped where each point refers to the RR interval (beat cycle length) of n^{th}+1 cardiac beat being plotted against n^{th} beat. Poincaré plots: Control (left), CYP2J2 KD (right). Poincaré plot descriptors (F) short term variability (STV_{RR}) and (G) long term variability (LTV_{RR}) define the extent of variability. Data provided was expressed as mean ± SD. Each point represents the measured parameter of a single cardiomyocyte cluster measured within a 30 s window. Boxplots depict the median of the datasets, the lower and upper quartiles and the minimum or maximum values within 1.5 × interquartile range from the lower and upper quartiles, respectively. Number of clusters measured: Control, $n = 62$; CYP2J2 KD (including all four individual treatment conditions), $n = 271$. Nonparametric Mann−Whitney *U* test was used to assess significant difference in the underlying data (****$P < 0.0001$). Analysis was performed using GraphPad Prism software v8.4.2 (San Diego, CA, USA).

results suggested the lack of torsadogenic potential of poyendarone. In summary, we have demonstrated that poyendarone preserves the anti-atrial fibrillatory properties while exhibiting significantly lower proarrhythmic risk in the canine model of persistent AF.

2.8. *Disclosure*

Aneesh V. Karkhanis, Gopalakrishnan Venkatesan, and Eric Chun Yong Chan hold patent titled 'Cardiac Therapeutic' describing the synthesis and use of poyendarone. Publication Number: WO2021006817, International Application Number: PCT/SG2020/050389.

3. Discussion

In this study, we aimed to investigate the role of CYP2J2 metabolism in drug-induced cardiac AEs. We judiciously designed a deuterated chemical probe, poyendarone, that fulfilled important chemical/biological criteria for investigating complex dronedarone-induced cardiac AEs. First, deuteration of dronedarone neither altered its physicochemical properties, hepatic and extrahepatic clearance nor multiple ion channel inhibitory pharmacology. Hence, poyendarone belongs to the same Biopharmaceutical Classification System Class II compound and Class III antiarrhythmic drug as dronedarone. These findings also suggested similar *in vivo* pharmacokinetics of dronedarone and poyendarone, which indeed

Table 3 Electrophysiological parameters in control (nonspecific siRNA) and CYP2J2 KD hESC-CMs.

Electrophysiological parameter	Control	CYP2J2 KD	Fold change (CYP2J2 KD/control)
Mean CTD (s)	1.440 ± 0.650	1.720 ± 0.805	1.19
Mean BTB (s)	1.586 ± 0.831	1.988 ± 1.238	1.25
BTB variability	0.146 ± 0.125	0.249 ± 0.276	1.71
STV_{RR} (ms)	152 ± 130	258 ± 321	1.70
LTV_{RR} (ms)	136 ± 124	217 ± 225	1.6

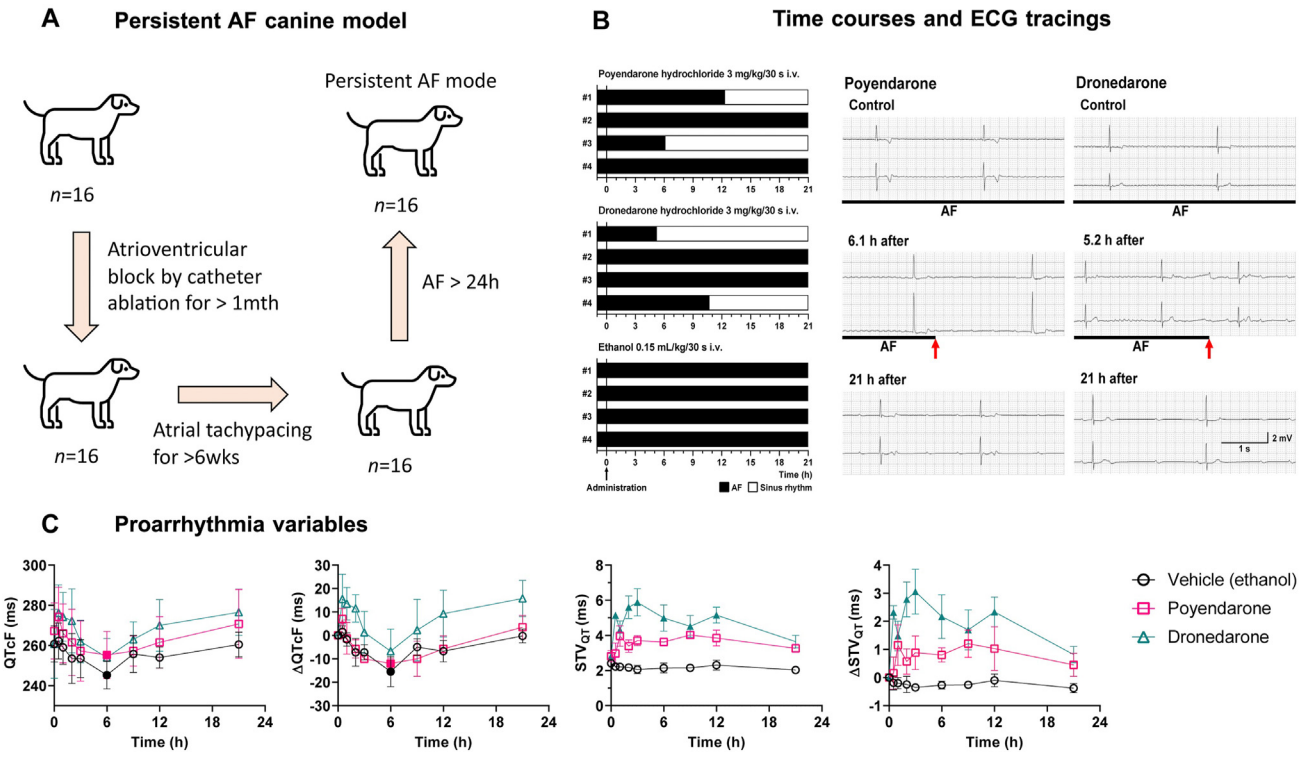

Figure 7 Poyendarone terminates persistent AF and exhibits lower torsadogenic risk. (A) Experimental plan for induction of atrioventricular block by catheter ablation and persistent AF by chronic atrial tachypacing at 600 bpm for more than 6 weeks in female beagle dogs. (B) Time courses of the anti-AF effects of poyendarone hydrochloride ($n = 4$), dronedarone hydrochloride ($n = 4$) and vehicle ethanol ($n = 4$). Anti-arrhythmic effects of poyendarone (left) and dronedarone (right) on the conscious dogs with persistent AF. Typical tracings of Holter electrocardiogram (NASA lead: upper; and CM5 lead: lower in each panel). Poyendarone and dronedarone terminated the persistent AF at 6.1 and 5.2 h after their administration, respectively (arrows). Thereafter, poyendarone and dronedarone maintained the sinus rhythm in the dogs until 21 h after their administration. (C) Time courses of changes in QTcF, ΔQTcF, STV_{QT} and ΔSTV_{QT} after poyendarone and dronedarone administration. Time courses of the anti-AF effects, typical tracings of Holter electrocardiogram and time courses of changes in proarrhythmia parameters of amiodarone are depicted in Fig. S10. The QT interval was corrected with Fridericia's formula: $QTcF = QT/(RR/1000)^{1/3}$ with RR given in ms[80]. The change in QTcF from its basal control at each time point was calculated (ΔQTcF). The STV_{QT} was calculated by following formula: $STV = \Sigma|QT_{n+1} - QT_n|/[50 \times \sqrt{2}]$. The change in STV_{QT} from its basal control at each time point was calculated (ΔSTV_{QT}). Data are presented as mean ± SEM ($n = 4$ per group for poyendarone, dronedarone and vehicle control). Filled symbols represent statistically significant differences ($P < 0.05$) from each control at specific time points while open symbols represent non-significant differences. Kruskal–Wallis test was used to assess statistical difference in the underlying data. Analysis was performed using GraphPad Prism software v8.4.2 (San Diego, CA, USA).

corroborated the results of our previous pharmacokinetic studies in healthy dogs[38]. The similar electrophysiological pharmacology further ensures that any rescue of drug-induced proarrhythmic effects of poyendarone is not strictly related to variable multiple ion channel inhibitory pharmacology.

Next, we demonstrated that deuteration of dronedarone exhibited substrate-dependence albeit significantly lower MBI of CYP2J2. Specifically, poyendarone either lacks MBI of CYP2J2 or exhibits dramatically lower potency in the MBI when rivaroxaban or astemizole was adopted as the probe substrate, respectively. The GSH trapping data further underlined that the benzofuran ring on the dronedarone molecule is susceptible to reactive metabolite formation and blocking of specific sites on the ring lowered or completely diminished the potency of CYP2J2 inactivation. Additionally, using differentially deuterated analogues of dronedarone, we confirmed that only deuteration on specific sites of the benzofuran ring is crucial for mitigating the MBI of CYP2J2 (data not shown).

In a previous study, dronedarone was found to cause MBI of CYP3A4 *via* two distinct mechanisms[35] *viz.* (1) dronedarone undergoes dealkylation to form *N*-desbutyldronedarone (NDBD) followed by hydroxylation to form reactive nitroso intermediate leading to metabolite-intermediate (MI) complex formation; (2) dronedarone undergoes desulfonation followed by quinone-oxime intermediate formation (same as observed for CYP2J2). Our previous results confirmed that dronedarone does not form nitroso intermediates or MI complexes with CYP2J2[13]. Hence CYP2J2 inactivation is primarily driven by quinone-oxime intermediate forming covalent adducts with enzyme active site. As *N*-alkyl chains were not deuterated in poyendarone, the dealkylation mechanism is not affected by the site-directed deuteration and therefore poyendarone retains inactivation effect against CYP3A4/5. Additionally, in a previous study, Schofield et al.[42] have shown that deuteration of *N*-alkyl chains does not prevent *N*-dealkylation reaction by CYP3A4/5. Hence the cardinal step of *N*-dealkylation and subsequent nitroso formation is resistant to deuteration. As a result, deuterating *N*-alkyl chains would have not resolved the MBI of CYP3A4/5. In conclusion, it is scientifically logical that poyendarone causes marginal MBI of CYP3A4/5 but not CYP2J2.

Finally, we also confirmed that poyendarone prevented CYP2J2-mediated AA metabolism inhibition and preserved the *in situ* EET levels. This result implies that mitigating the MBI of CYP2J2 preserves its AA-EETs metabolism activity. Hence, the toxicological differences between the two drugs are attributed to preservation of the AA-EET metabolic axis. Our laboratory has previously reported that EET enrichment rescued cardiomyocytes from dronedarone-induced mitochondrial toxic insults *via* activation of mitoK$_{ATP}$ channels which in turn preserved mitochondrial membrane potential, hindered mitochondrial permeability transition pore opening, reduced ATP loss, and prevented cell death[24]. In corroboration, we demonstrated that poyendarone preserved CYP2J2 epoxygenase activity and EET levels *in vitro* and therefore alleviated mitochondrial toxicity in cardiomyocytes.

EETs not only prevent mitochondrial toxicity but also modulate several cardiac ion channels. For instance, EETs enhance $I_{Ca,L}$ currents *via* cAMP/PKA pathway and activate the ATP sensitive-K^+ (K_{ATP}) channels by reducing the channel sensitivity to ATP in rat cardiomyocytes[7,43]. Transgenic mice with cardiac-specific CYP2J2 overexpression and subsequent elevated intracardiac EET levels, exhibit enhanced cardiac $I_{Ca,L}$, K_{ATP}, transient outward $K^+_{(I_{to})}$ currents, and shortened cardiac action potential duration without incidences of arrhythmogenesis or sudden cardiac death[44]. In parallel, cardiac-specific CYP2J3/10$^{-/-}$ transgenic rats (rat isoforms of human CYP2J2) exhibited 75% loss in metabolic activity and 66.6% reduction in *in vivo* probe substrate clearance compared to WT rats[45]. Additionally, creatine kinase-muscle brain type, serum creatine kinase and their ratio were considerably increased indicative of myocardial injury and cardiomyocyte damage[46]. In a separate report, CYP2J2 silencing in adult human ventricular cardiomyocytes revealed significant transcriptional modulation of the genes associated with cardiac remodeling and ion channel signaling pathways, with roles in cardiomyopathies and arrhythmias[47]. In both studies, CYP2J2 deletion was not associated with sudden cardiac death in rats or excessive cell death in human cardiomyocytes. The researchers opined that after CYP2J2 deletion, a second pathophysiological "hit" may be essential to observe cardiac AEs[47]. Our findings confirmed that both dronedarone-mediated inhibition and genetic knockdown of CYP2J2 increased parameters related to BTB variability, underscoring the direct role of CYP2J2 in heart rhythm control. Conversely, the preservation of CYP2J2 metabolism by poyendarone decreased BTB variability significantly. Taken together, we postulate that the second "hit" may manifest in the form of drug inhibition of CYP2J2 thus compounding drug-induced proarrhythmic effects leading to fatal consequences.

Previously, we replicated anti-atrial fibrillatory effects of dronedarone and poyendarone in healthy[38,39] and paroxysmal AF dogs[40]. Dronedarone delayed atrioventricular (AV) and intraventricular (IV) conduction and ventricular repolarization and displayed moderate atrial selectivity. Interestingly, poyendarone displayed 1.7-fold greater atrial selectivity compared to dronedarone in addition to the delays in AV and IV conduction[38,39]. Dronedarone also significantly prolonged the phase-3 repolarization period possibly due to modest induction of Ca^{2+} overload while poyendarone hardly altered phase-3 repolarization period suggesting a lack of Ca^{2+} overload[48]. It has been reported that the prolongation of the terminal repolarization period leads to conduction delay at an incomplete repolarization level leading to reentry arrhythmia occurs, which is associated with a high drug-induced torsadogenic risk[44]. Here, we further investigated the relative effects of poyendarone in persistent AF canine model which was prepared by chronic atrial tachypacing (600 bpm for >6 weeks) of the standard chronic atrioventricular block dog model. This model has been extensively employed in cardiovascular research on drug-induced TdP which is in line with clinical observations[49]. Initially, vehicle ethanol failed to terminate the persistent AF, confirming that the cardioversion of AF observed after the administration of the drugs would depend on their cardiac electrophysiological actions. Since 3 mg/kg, i.v. of poyendarone suppressed AF in the paroxysmal AF model dogs[40], we selected the dose in this study to assess its anti-AF effect on the persistent AF canine model. Like dronedarone, poyendarone terminated the AF in 2 out of 4 animals, resulting in sinus rhythm (50%). These findings are consistent with the similar *in vitro* electrophysiological pharmacology of the compounds. To further characterize anti-AF efficacy of poyendarone, we compared its effects with amiodarone[50] on the surrogate markers of anti-AF action such as inter-atrial conduction time and atrial effective refractory period in canine model of paroxysmal AF. At a basic pacing cycle length of 200 ms, simulating the electrophysiological condition in atria during AF[40,49] the potency for the inter-atrial conduction time prolongation was in the order of poyendarone (+13 ms)=dronedarone (+13 ms) > amiodarone (+1 ms), whereas that for the atrial effective refractory period prolongation was in the order of poyendarone (+9 ms) > dronedarone (+4 ms) > amiodarone (−3 ms), which could at least in part explain the recurrence of AF in one animal after amiodarone administration (#1 in Figs. S10A and B). These observations also support the comparable anti-AF potency between poyendarone and dronedarone against the persistent AF canine model in this study. Importantly, lethal ventricular arrhythmia such as TdP or hemodynamic collapse was not observed during the experimental period, indicating a favorable cardiac safety profile of each drug at their anti-AF dose.

To compare the proarrhythmic potential of the drugs quantitatively, we assessed the QTcF as well as STV_{QT} which is a highly specific and sensitive marker for drug-induced proarrhythmia. Although QT prolongation is traditionally used to predict torsadogenic risk, STV_{QT} was proven to be a superior parameter[51]. Moreover, its utility has been established in several pre-clinical and clinical studies[52–54]. In our study, the potency for the ΔQTcF prolongation was in the order of dronedarone > poyendarone ≥ amiodarone, indicating that the effect of dronedarone on repolarization period could be attenuated by the deuteration. Meanwhile, the extent of increase in the STV_{QT} was in the order of dronedarone > poyendarone ≥ amiodarone, indicating that propensity of poyendarone to cause BVR was lower than dronedarone *in vivo*. This observation supports the hypothesis that poyendarone has a lower proarrhythmic risk than dronedarone and preservation of CYP2J2 metabolism plays a role in drug-induced proarrhythmia.

Our work has provided novel mechanistic insight into the role of CYP2J2 in drug-induced cardiac AEs and proarrhythmia. Several marketed drugs such as ketoconazole & itraconazole (antifungal), doxorubicin and imatinib (anticancer) and nortriptyline (antidepressant) cause or exacerbate heart failure possibly by inducing ventricular tachycardia and potently inhibit CYP2J2 *in vitro*[55]. We propose that CYP2J2 must be explored as a possible novel toxicity target and could be incorporated into the Comprehensive *In Vitro* Proarrhythmia Assay testing framework[56]. More importantly, specific CYP2J2 inhibitors being developed as novel anticancer drugs such as compound C26 must be evaluated for its torsadogenic propensity[30].

Association of CYP2J2 polymorphisms with cardiovascular diseases has been recently explored. CYP2J2*7 is one of the most common polymorphisms with allelic frequency varying greatly with ethnicity (1.1%−1.2% in Caucasian, 2.6% in Chinese, and 11%−17% in African populations)[57]. CYP2J2*7 polymorphism due to substitution of G>T in the CYP2J2 promoter region results in 48% loss in promoter activity and 30% lower serum EET levels[57,58]. Interestingly, CYP2J2*7 incidence positively correlates to the risk of coronary artery disease and myocardial infarction in specific populations[58,59]. However, there are no studies exploring the distribution of CYP2J2*7 and its pathological implications in AF patients. In such patients, lower basal EET levels might serve as a torsadogenic substrate and hence poyendarone may be more suited anti-AF therapy than dronedarone due to negligible BVR. Moreover, screening patients for CYP2J2*7 expression would prove to be a useful strategy for personalized AF treatment.

Lastly, although deuteration is an established approach to improve the pharmacokinetic and toxicological properties of drugs; it was only recently that USFDA granted accelerated regulatory approval to the first deuterated drug, deutetrabenazine (Austedo®)[60,61]. This has renewed interest in deuteration strategies and spurred the development of several drug candidates[61]. Accelerated approval for deutetrabenazine was possibly based on previous safety studies of the approved, parent, nondeuterated drug, tetrabenazine[60]. Contrary to traditional drug development timelines, this regulatory change may significantly shorten the clinical drug development timeline and save enormous costs. In light of this progress, further efficacy and safety studies of poyendarone could be performed first in animal models of permanent AF and decompensated heart failure[49] followed by in a targeted cohort of patients. Past preclinical and clinical studies of dronedarone coupled with selected trials of poyendarone may facilitate poyendarone's regulatory approval for a safe and efficacious pharmacotherapeutic management of AF.

4. Conclusions

Cardiac AEs precipitated by dronedarone in terms of mitochondrial toxicity, increased BTB in cardiomyocytes and higher proarrhythmic risk in persistent AF models are attributed to MBI of CYP2J2 and depletion of *in vivo* EET levels. Here we designed poyendarone, a deuterated analogue of dronedarone, that circumvents CYP2J2 inactivation, preserves AA-EET metabolism and mitigates both dronedarone-induced mitochondrial toxicity and proarrhythmia in cardiomyocytes. Poyendarone further preserves antiarrhythmic pharmacology while it significantly reduces proarrhythmic risk in persistent atrial fibrillation dogs. In conclusion, the preservation of functional CYP2J2 activity prevents dronedarone-induced cardiac AEs. Moreover, poyendarone is a potentially novel, safe, and efficacious antiarrhythmic drug.

5. Experimental

5.1. Synthesis of poyendarone

Chemicals. All reagents except poyendarone were of analytical grade and purchased from Sigma−Aldrich (St. Louis, MO, USA) unless otherwise mentioned. HPLC-grade acetonitrile (ACN) was purchased from Tedia Company Inc. (Fairfield, OH, USA). Water was obtained using a Milli-Q water purification system (Millipore, Billerica, MA, USA). Poyendarone was synthesized as described in the supplementary file (Supporting Information Fig. S2).

Briefly, all synthetic reactions were routinely monitored by thin-layer chromatography (TLC) on silica gel plate (precoated 60 F_{254} Merck plate). Column chromatography was performed using silica gel 60 (Merck, 70−230 mesh). Compounds were dissolved in HPLC grade methanol for determination of mass to charge (*m*/*z*) using the AB Sciex 2000 mass spectrometer with electrospray ionization (ESI). ^{1}H NMR spectra were determined in deuterated chloroform ($CDCl_3$) and deuterated dimethyl sulfoxide (DMSO-d_6) solutions on Bruker DPX Ultrashield NMR spectrometer (400 MHz), with chemical shifts given in parts per million (δ) downfield relative to tetramethylsilane (TMS) as internal standard, and *J* values (coupling constants) given in hertz. The following abbreviations were used: s, singlet; d, doublet; t, triplet; p, pentet; sxt, sextet; m, multiplet. The synthesis scheme is shown in Fig. S2.

5.1.1. 2-(Bromomethyl)-4-nitrophenol(3,5,6-d_3) (**D1**)

Concentrated sulfuric acid (0.121 mL) was added to a mixture of 4-nitro(2,3,5,6-d_4)phenol (1.25 g, 8.73 mmol/L) and 48% HBr solution (15.8 mL) at room temperature, followed by 35% formalin solution (0.760 g, 24.4 mmol/L, 2.8 eq). The reaction mixture was heated at 75 °C with stirring for 6 h. Following which the reaction mixture was poured slowly into ice water mixture and stirred for 1 h. The obtained solid was filtered, washed with cold water and then dried under vacuum to obtain a beige solid. Toluene (50 mL) was added to the solid and the mixture was heated with stirring at 85 °C for 1 h. The mixture was cooled to 5 °C and stirred for 1 h at the same temperature. The resulting solid was filtered, washed with toluene and then dried under vacuum to get a white solid as the product. Yield: 76.5%, ^{1}H NMR (400 MHz, DMSO-d_6): δ 4.70 (s, 2H), 11.61 (s, 1H). The ^{1}H NMR spectrum of the synthesized product is shown in Fig. S2A.

5.1.2. 2-((Bromotriphenylphosphoranyl)methyl)-4-nitrophenol(3,5,6-d_3) (**D2**)

To a solution of 1.5 g (6.38 mmol/L) of 2-(bromomethyl)-4-nitrophenol(3,5,6-d_3) (**D1**) in toluene (10 mL) was added 1.67 g of triphenyl phosphine (6.38 mmol/L) and the mixture was refluxed for 1 h. After completion of the reaction, the mixture was cooled, and the resulting precipitate was filtered. The filtrate was evaporated to dryness and stirred with toluene (10 mL) for 30 min and filtered to obtain a solid. Both solids were combined and dried under vacuum to obtain a white solid. Yield: 99.0%, ^{1}H NMR (400 MHz, $CDCl_3$): δ 4.76−4.80 (d, J = 14.0 Hz, 2H), 7.57−7.66 (m, 12H), 7.78−7.82 (m, 3H). The ^{1}H NMR spectrum of the synthesized product is shown in Fig. S2B.

5.1.3. 2-Butyl-5-nitro-1-benzo(4,6,7-d_3)furan (**D3**)

To a solution of 1.65 g (3.32 mmol/L) of 2-((bromotriphenylphosphoranyl)methyl)-4-nitrophenol(3,5,6-d_3) (**D2**) in 10 mL of $CHCl_3$ was added 0.522 g (6.6 mmol/L, 2 eq) of pyridine. 0.500 g (4.05 mmol/L, 1.25 eq) of valeroyl chloride was slowly added to the mixture with stirring at room temperature. The mixture was refluxed for 2 h and then 25 mL of toluene was added and about half of the solvent was evaporated under reduced pressure. 1.0 g (9.96 mmol/L, 3 eq) of triethylamine was then added and refluxed for a further 3 h. The resulting reaction mixture was cooled and the triphenyl phosphine oxide formed was filtered, washed with ethyl acetate and the filtrate was

concentrated under vacuum. The viscous residue formed was purified by column chromatography using petroleum ether: ethyl acetate (95:5) to obtain a colorless residue. Yield: 73.5%, ^{1}H NMR (400 MHz, $CDCl_3$): δ 0.85−0.89 (t, J = 7.20 Hz, 3H), 1.28−1.38 (m, 2H), 1.70−1.78 (m, 2H), 2.87−2.91 (t, J = 7.60 Hz, 2H), 7.53−7.55 (d, J = 8.80 Hz, 1H). The ^{1}H NMR spectrum of the synthesized product is shown in Fig. S2C.

*5.1.4. (2-Butyl-5-nitro-1-benzo(4,6,7-d_3)furan-3-yl)(4-methoxyphenyl)methanone (**D4**)*

To a solution of 2-butyl-5-nitro-1-benzo(4,6,7-d_3)furan (**D3**) (1.4 g, 6.29 mmol/L) in 15 mL dichloromethane was slowly added 4-methoxybenzoyl chloride (1.61 g, 9.45 mmol/L, 1.5 eq) and tin(IV) chloride (4.1 g, 15.7 mmol/L, 2.5 eq) over 1 h at 0−5 °C and stirring was continued for 24 h at room temperature. The reaction mixture was cooled at 0−5 °C following which water (10 mL) was added slowly and the mixture was stirred for about 30 min. The aqueous layer was separated and extracted with dichloromethane (3 × 10 mL). The combined organic layer was evaporated under reduced pressure. The crude compound obtained was purified by column chromatography using petroleum ether: ethyl acetate (85:15) to obtain a white solid as product. Yield: 93.5%, ^{1}H NMR (400 MHz, $CDCl_3$): δ 0.86−0.89 (t, J = 7.40 Hz, 3H), 1.29−1.38 (m, 2H), 1.71−1.78 (m, 2H), 2.88−2.92 (t, J = 7.60 Hz, 2H), 3.90 (s, 3H), 6.96−6.99 (d, J = 8.80 Hz, 2H), 7.80−7.83 (d, J = 8.80 Hz, 2H). The ^{1}H NMR spectrum of the synthesized product is shown in Fig. S2D.

*5.1.5. 2-Butyl-5-nitro-1-benzo(4,6,7-d_3)furan-3-yl)(4-hydroxyphenyl)methanone (**D5**)*

To a solution of 1.02 g (2.86 mmol/L) of (2-butyl-5-nitro-1-benzo(4,6,7-d_3)furan-3-yl)(4-methoxyphenyl)methanone (**D4**) in dichloromethane (50 mL) was added $AlCl_3$ (2.29 g, 17.2 mmol/L, 6 eq) slowly over 1 h with stirring at 0−5 °C. The mixture was refluxed for 24 h and cooled to room temperature and subsequently to 0−5 °C. Water (10 mL) was added slowly and the mixture was stirred for about 30 min. The organic layer was separated and concentrated under vacuum to give a residue which was purified by column chromatography using petroleum ether: ethyl acetate (90:10) to obtain a yellowish oil. Yield: 98.0%, ^{1}H NMR (400 MHz, $CDCl_3$): δ 0.87−0.90 (t, J = 7.20 Hz, 3H), 1.30−1.39 (m, 2H), 1.72−1.80 (m, 2H), 2.90−2.94 (t, J = 7.60 Hz, 2H), 6.94−6.96 (d, J = 8.80 Hz, 2H), 7.77−7.80 (d, J = 8.80 Hz, 2H). The ^{1}H NMR spectrum of the synthesized product is shown in Fig. S2E.

*5.1.6. 2-Butyl-5-nitro-1-benzo(4,6,7-d_3)-furan-3-yl)(4-(3-(dibutylamino)propoxy)phenyl)methanone (**D6**)*

To a solution of 0.800 g (2.3 mmol/L) of (2-butyl-5-nitro-1-benzo(4,6,7-d_3)furan-3-yl)(4-hydroxyphenyl)methanone (**D5**) in 20 mL of acetone was added 3.23 g (2.3 mmol/L, 1 eq) of anhydrous K_2CO_3 and 4.79 g (2.3 mmol/L, 1 eq) of 1-chloro-3-di-*n*-butylaminopropane at room temperature. The reaction mixture was refluxed at 60 °C overnight. The reaction mixture was cooled and evaporated under reduced pressure. To the resulting solid, water (20 mL) was added and stirred for 5 min and extracted with dichloromethane (3 × 20 mL). The organic layer was evaporated under reduced pressure to obtain a crude residue which was further purified by column chromatography using petroleum ether: ethyl acetate (70:30) to obtain a yellowish oily residue. Yield: 77.0%, ^{1}H NMR (400 MHz, DMSO-d_6): δ 0.80−0.84 (m, 9H), 1.22−1.27 (m, 6H), 1.30−1.37 (m, 4H), 1.64−1.72 (m, 2H), 1.82−1.85 (t, J = 6.40 Hz, 2H), 2.33−2.36 (t, J = 7.00 Hz, 4H), 2.51−2.53 (m, 2H), 2.82−2.86 (t, J = 7.60 Hz, 2H), 4.12−4.15 (t, J = 6.00 Hz, 2H), 7.08−7.10 (d, J = 8.80 Hz, 2H), 7.81−7.83 (d, J = 8.80 Hz, 2H). The ^{1}H NMR spectrum of the synthesized product is shown in Fig. S2F.

*5.1.7. 5-Amino-2-butyl-1-benzo(4,6,7-d_3)-furan-3-yl)(4-(3-(dibutylamino)propoxy)phenyl)methanone (**D7**)*

A mixture of 0.114 g (0.22 mmol/L) of (2-butyl-5-nitro-1-benzo(4,6,7-d_3)furan-3-yl)(4-(3(dibutylamino)propoxy)phenyl) methanone (**D6**), 0.106 g (1.33 mmol/L, 6 eq) of iron powder, 0.5 mL of ethanol and 0.25 mL of water was stirred at room temperature for 10 min. The reaction mixture was cooled to 15 °C and 0.5 mL of concentrated HCl was added. The reaction mixture was stirred for 3 h at 65 °C, cooled, poured into ice water mixture and stirred for 30 min. The aqueous layer was extracted with dichloromethane (3 × 5 mL). The pH of the organic layers was adjusted to 8−9 using aqueous ammonia solution. Both the organic and aqueous layers were separated. The aqueous layer was extracted with dichloromethane (3 × 5 mL) and both the organic layers were combined, dried with Na_2SO_4 and removed under reduced pressure to obtain a colorless oil. Yield: 80.3%, ^{1}H NMR (400 MHz, $CDCl_3$): δ 0.87−0.91 (m, 9H), 1.25−1.37 (m, 6H), 1.42−1.49 (m, 4H), 1.71−1.79 (m, 2H), 1.99−2.02 (m, 2H), 2.47−2.50 (m, 4H), 2.65−2.69 (m, 2H), 2.89−2.93 (t, J = 7.60 Hz, 2H), 4.11−4.14 (t, J = 6.20 Hz, 2H), 6.96−6.98 (d, J = 8.80 Hz, 2H), 7.80−7.82 (d, J = 8.80 Hz, 2H). The ^{1}H NMR spectrum of the synthesized product is shown in Fig. S2G.

*5.1.8. Methanesulfonamide, N-(2-butyl-3-(4-(3-(dibutylamino) propoxy)benzoyl)-1-benzo(4,6,7-d_3)-furan-5-yl)hydrochloride (**D8**)*

To a warmed solution of 0.100 g (0.207 mmol/L) of (5-amino-2-butyl-1-benzo(4,6,7-d_3)furan-3-yl)(4-(3-(dibutylamino)propoxy) phenyl) methanone (**D7**) in anhydrous dichloromethane (3 mL) was added 0.0197 g (0.249 mmol/L, 1.2 eq) of pyridine and 0.028 g (0.249 mmol/L, 1.2 eq) of methane sulfonylchloride slowly over 5 min at 35 °C. The resulting mixture was stirred at the same temperature for 3 h and then cooled to room temperature. This mixture was then washed with 2 × 5 mL of water, 2 × 5 mL of 5% $NaHCO_3$ solution and 1 × 5 mL of water. The organic phase was separated and concentrated, which was further purified by column chromatography using petroleum ether: ethyl acetate (10:90) to obtain a brown oily residue in 80% yield. To this residue 5 mL of methanol was added and a solution of hydrochloric acid (0.100 mL) in 0.4 mL of methanol was added over 20 min. The reaction mixture was stirred for 3 h at 0 °C and the obtained solid was filtered and washed with methanol and dried to obtain the final compound (poyendarone) as pale brown solid. ESI-MS (m/z) calculated for $C_{31}H_{41}D_3N_2O_5S$ $[M+H]^+$ 559.77. Yield: 79.0%, overall yield: 25.0%, ^{1}H NMR (400 MHz, MeOH-d_4): δ 0.83−0.88 (m, 3H), 0.89−0.93 (t, J = 7.20 Hz, 6H), 1.27−1.33 (m, 6H), 1.43−1.47 (m, 4H), 1.69−1.77 (m, 2H), 1.94−1.99 (m, 2H), 2.45−2.49 (m, 4H), 2.64−2.68 (t, J = 7.40 Hz, 2H), 2.86−2.89 (t, J = 7.60 Hz, 2H), 2.96 (s, 3H), 4.12−4.16 (t, J = 6.00 Hz, 2H), 7.03−7.06 (d, J = 8.8 Hz, 2H), 7.78−7.87 (d, J = 9.2 Hz, 2H), ^{13}C NMR (400 MHz, MeOH-d_4): 13.7, 19.5, 20.7, 23.2, 24.7, 26.7, 28.7, 31.1, 38.8, 51.2, 54.0, 66.3, 115.6, 117.9, 128.9, 129.7, 132.3, 132.7, 133.3, 135.5, 152.7, 163.9, 165.5, 167.5, 192.5. The ^{1}H and ^{13}C NMR spectrum of the synthesized product is shown in Figs. S2H and S2I, respectively. HPLC purity (254 nm); 98.4%, eluent: 60% acetonitrile/0.1%

formic acid in water, T_R = 4.6 min (Fig. S2J). The ^1H and ^{13}C NMR spectra of dronedarone are shown in Fig. S2K and S2L, respectively.

5.2. Determination of lipophilicity, aqueous solubility, permeability, and in vitro metabolic stability

5.2.1. Lipophilicity calculation

Lipophilicity or the computational log *P* values (*c*log*P*) of poyendarone and dronedarone were estimated using ChemSketch software (ACD Labs v2020.1.2).

5.2.2. Aqueous solubility determination

Aqueous kinetic solubilities of poyendarone and dronedarone were determined using Multiscreen PCF filter plates (Millipore). 10 μL of 10 mmol/L stock solution of poyendarone or dronedarone was added to the universal aqueous buffer, pH 7.4 (1% DMSO, *v*/*v*), and sonicated. 300 μL of the mixture was transferred to the 3 wells of MultiScreen $_{HTS}$-PCF filter plate and agitated for 24 h at 250 rpm at room temperature and filtered. After filtration, ACN was added to the filtrate to give 80:20 buffer/ACN composition and the UV absorbance was determined at 300 nm to give an estimate of aqueous solubility.

5.2.3. Effective permeability measurement

Effective permeability of test compounds was determined by Parallel Artificial Membrane Permeability Assay (PAMPA) using Multiscreen-IP PAMPA and Receiver plates (Millipore). 1% *w*/*v* solution of lecithin in dodecane and 300 μL of 10-fold diluted solution (prepared in 1× PBS buffer) of poyendarone and dronedarone were applied to donor plate. An equal volume of 1× PBS buffer was added to the corresponding well in the acceptor plate. The donor/acceptor plate unit was placed in an air-tight container and agitated for 16 h, 250 rpm at room temperature. 250 μL/well of solution of donor wells and acceptor wells were transferred to separate wells in a 96-well UV plate and UV absorbance was measured at 300 nm. Similarly, the permeability of standard compounds namely caffeine, carbamazepine, quinidine, verapamil, warfarin, and propranolol were measured. The absorbance of the solutions was determined at λ_{max} of the standard compound on a microplate reader (caffeine 296 nm, carbamazepine 316 nm, quinidine 330 nm, verapamil 290 nm, warfarin 336 nm, propranolol 300 nm).

5.2.4. Metabolic stability assays

The metabolic stability experiments were performed to derive intrinsic clearance (CL_{int}) values *via* the substrate depletion method as described before[13,35]. Briefly, 1 μmol/L dronedarone or poyendarone was incubated with the HLM (0.5 mg/mL), rCYP2J2 (20 pmol/mL), rCYP3A4 (10 pmol/mL) or rCYP3A5 (10 pmol/mL) and NADPH generating system consisting of NADPH A (NADP+ and glucose 6-phosphate) and B (glucose-6-phosphate dehydrogenase) (BD Gentest, Woburn, MA, USA). At specific time points, aliquots were collected and quenched using ice-cold ACN with internal standard (IS) and the parent compound was analyzed with liquid chromatography-tandem mass spectrometry (LC−MS/MS). CL_{int} was determined by plotting percentage substrate remaining against incubation time and fitting to one-phase decay model as described previously[1].

5.3. Whole-cell patch clamp measurement in transfected HEK293FT cells

Cell culture. HEK293FT cells (ATCC, Manassas, VA, USA) were cultured in DMEM (Thermo Fisher Scientific) supplemented with 10% fetal bovine serum (FBS) and 1% penicillin and streptomycin and maintained in 5% CO_2 incubator at 37 °C. For transfection, cells were seeded on the petri dishes containing coverslips and grown overnight.

5.3.1. Measurement of $Na_v1.5$ current

Cells were co-transfected with 3.0 μg of human $Na_V1.5$ channel plasmid and 1.5 μg of human auxiliary $\beta1$ subunit plasmid by lipofectamine 2000 (Thermo Fisher Scientific)[62]. The cells were grown for 24 h in 5% CO_2 incubator at 37 °C, split and seeded on poly-D coated coverslip 24 h before patch clamp analysis. To record $Na_V1.5$ current, the internal solution (pipette solution) contained (in mmol/L) 130 CsF, 5 NaCl, 5 EGTA, 10 HEPES, 2 $MgCl_2$, 2 TEA-Cl pH 7.2 (adjusted with CsOH). The external solution contained (in mmol/L): 135 NaCl, 4.2 CsCl, 1.2 $MgCl_2$, 1.8 $CaCl_2$, 10 HEPES and glucose, adjusted to pH 7.4 with NaOH. Cells were treated with increasing concentrations of poyendarone or dronedarone (1−10 μmol/L). Whole cell currents were obtained under voltage clamp with an Axopatch200B or Multiclamp 200B amplifier (Molecular Device, San Jose, CA, USA), low-pass filtered at 5−6 kHz and the series resistance was typically <5 MΩ after >70% compensation. The P/4 protocol was used to subtract online the leak and capacitive transients. Dose-response curve was fitted with log(inhibitor) *vs* response variable slope as Eq. (1):

$$Y = \text{Bottom} + \frac{(\text{Top} - \text{Bottom})}{\left(1 + 10^{(\text{LogIC50} - X) \times \text{Hill Slope}}\right)} \quad (1)$$

5.3.2. Measurement of $Ca_v1.2$ current

Cells were co-transfected with 1.7 μg of human $Ca_V1.2$ α_{1C} cardiac isoform (1a/8a splice variant) and 1.25 μg of human auxiliary β_2 and α_2/δ_1 subunits by lipofectamine 2000[63,64]. The cells were grown for 24 h in 5% CO_2 incubator at 37 °C, split and seeded on poly-D coated coverslip 24 h before patch-clamp analysis. To record $Ca_V1.2$ current the internal solution (patch-pipette solution) contained the following (in mmol/L): 138 Cs-$MeSO_3$, 5 CsCl, 5.0 EGTA, 10 HEPES, 1 $MgCl_2$, 2 mg/mL Mg-ATP, pH 7.3 (adjusted with CsOH), 290 mOsm with glucose. The external solution contained the following (in mmol/L): 10 HEPES, 140 tetraethylammonium methanesulfonate, 5 $CaCl_2$ (pH adjusted to 7.4 with CsOH and osmolality to 290−310 with glucose). Pipettes of resistance 1.5−2 MΩ were used. Cells were treated with increasing concentrations of poyendarone (1−5 μmol/L) or dronedarone (1−5 μmol/L). Dose−response curve was fitted with log(inhibitor) *vs* response variable slope Eq. (1).

5.3.3. Measurement of $K_V11.1$ current

Cells were co-transfected with 2 μg of $K_V11.1$ channel plasmid and 1 μg of KCNE1 plasmid by lipofectamine 2000[65]. The transfected cells were incubated for 24 h in 5% CO_2 incubator at 37 °C 48 h post transfection, the cells were split and seeded on poly-D lysine coverslip one day before recording. To record $K_V11.1$ current, the internal solution (pipette solution) contained (in mmol/L) 130 K-gluconate, 10 KCl, 5 EGTA, 10 HEPES, 1 $MgCl_2$, 0.5

Na_3GTP, 4 Mg-ATP, Na-phoshocreatine pH 7.4 (adjusted with KOH). The external solution contained (in mmol/L): 125 NaCl, 2.5 KCl, 25 Na-gluconate, 1.0 $MgCl_2$, 1.8 $CaCl_2$, 10 HEPES and 11.1 glucose, adjusted to pH 7.4 with NaOH. Cells were treated with increasing concentrations of poyendarone (10 nmol/L−1 μmol/L) or dronedarone (10 nmol/L−1 μmol/L). Whole cell currents were obtained under voltage clamp with an Axopatch200B or Multiclamp 200B amplifier, low-pass filtered at 1 kHz and the series resistance was typically <5 MΩ after >70% compensation. The P/4 protocol was used to subtract online the leak and capacitive transients The $K_v11.1$ current was evoked from holding potential of −80 mV to 2.5 s pulses of 20 mV. The tail currents were subsequently recorded upon returning the voltage to −60 mV. Dose-response curve was fitted with log(inhibitor) *vs* response variable slope as Eq. (1).

5.4. MBI of CYP2J2, CYP3A4 or CYP3A5

Time- and concentration-dependent inactivation of CYP2J2, CYP3A4 and CYP3A5 by poyendarone or dronedarone was determined using the two-step incubation method as described before[35]. Briefly, primary mixtures comprising dronedarone or poyendarone (0−20 μmol/L) were incubated with rCYP2J2, rCYP3A4 or rCYP3A5 (20 pmol/mL) and NADPH B in potassium phosphate buffer and reaction was initiated with NADPH A. At different pre-incubation time points at 37 °C, aliquots were transferred to a secondary incubation mixture consisting of rivaroxaban and NADPH regenerating system resulting in 10- or 20-fold dilution for CYP2J2 or CYP3A4/5 respectively. The secondary mixtures were incubated for 30 min with CYP2J2 or 2 h with CYP3A4/5. Reaction mixtures were quenched with ice-cold ACN with IS and centrifuged. The supernatants were analyzed for morpholinone moiety of rivaroxaban using LC−MS/MS as described before[66]. CYP2J2 inactivation was separately confirmed using another probe substrate astemizole as described previously[13]. MBI parameters such as the maximum inactivation rate constant (k_{inact}) and inactivator concentration at half-maximum inactivation rate constant (K_I) were determined as described previously[13]. The k_{inact}/K_I ratio measures the potency of MBI where higher the k_{inact}/K_I ratio, the more potent is the enzyme inactivation.

5.4.1. GSH trapping assay

Incubation mixtures containing 500 pmol/mL rCYP2J2, 50 μmol/L poyendarone or dronedarone NADPH B, 100 mmol/L potassium phosphate buffer (pH 7.4) and 50 mmol/L reduced L-glutathione (GSH) were pre-incubated for 5 min and NADPH A was added to initiate the reaction. The final volume of incubation mixture was 500 μL and three replicates of the incubation mixtures were prepared for each test compound. After 60 min of incubation at 37 °C, 500 μL of ice-cold ACN was added to quench the reaction. The solutions were centrifuged at 16,000×*g* at 4 °C for 15 min. The supernatant was pooled and evaporated under the gentle stream of nitrogen using TurboVap LV (Caliper Life Science, Hopkinton, MA). The residue was reconstituted with 60 μL 3:7 *v/v* ACN-water mixture. The mixtures were vortexed for 5 min and centrifuged 16,000×*g* at 4 °C for 15 min and the supernatant was extracted for LC−MS/MS analysis as described before[13]. Negative control experiments were performed without the presence of test compounds.

5.5. Inhibition of CYP2J2-mediated AA metabolism

AA, 5,6-EET, 8,9-EET, 11,12-EET, 14,15-EET were purchased from (Cayman Chemical, Ann Arbor, MI, USA). Assay for inhibition of CYP2J2-mediated AA metabolism by poyendarone or dronedarone was carried out as published before[25]. Briefly, CYP2J2, AA and poyendarone or dronedarone were co-incubated with NADPH (Nacalai Tesque, Kyoto, Japan) for 2 h, the reaction mixture was then quenched with ice-cold ACN, and centrifuged. The EETs were measured in the supernatant using LC−MS/MS. Inhibition of AA metabolism was determined as reduced EET formation and represented as percentage control (no inhibitor).

5.6. In vitro cardiac mitochondrial toxicity assays

5.6.1. Concurrent measurement of cytotoxicity and ATP depletion in cardiac cells

Rat cardiac cells, H9c2 (ATCC), were cultured in low glucose DMEM and differentiated with all-*trans* retinoic acid according to established protocols[67]. The cytotoxicity and intracellular ATP depletion were measured concurrently in differentiated rat cardiac H9c2 cells on treatment with poyendarone or dronedarone with Mitochondrial ToxGlo™ kit (Promega, Madison, WI, USA) according to manufacturer's protocol.

5.6.2. Oxygen consumption in isolated rat heart mitochondria

Healthy male Wistar Han rats were housed at the National University of Singapore (NUS) animal facility in a 12 h light/day cycle. Animal chow and water were provided *ad libitum*. The animals were sacrificed and rat hearts were isolated according to ethical regulations of the NUS Institutional Animal Care and Use Committee (Protocol No: R15-0027). The mitochondria from freshly resected whole heart were isolated using published protocol[68]. The mitochondrial protein was measured using Pierce™ BCA protein assay kit (Thermo Fisher Scientific). The purity of the isolated mitochondria was assessed with citrate synthase assay[69].

The OCR is reflective of mitochondrial complex I and II activity when supplemented with specific respiratory substrates such as NADH and succinate respectively. The activity of ETC was assessed using the Clarke-type oxygen electrode. Mitochondrial suspension was co-treated with NADH (1 mmol/L) and succinate (4 mmol/L) and poyendarone or dronedarone (1−100 μmol/L). Rotenone (0.5 μmol/L) and malonic acid (0.5 mmol/L) were used as positive control inhibitors of complex I and II respectively. Percentage saturation was measured and extent of inhibition of the complexes was reported as percentage of control (only substrate) values as described previously[24].

5.7. In vitro assessment of drug induced CYP2J2 inhibition on cardiac BTB variability

5.7.1. Cell culture

Human foreskin fibroblasts (Lonza, Basel, Switzerland) were reprogrammed to form human induced pluripotent stem cells (hiPSC) using a viral-free method and differentiated to cardiomyocytes as described in published reports[70]. CYP2J2 gene

expression was quantified with RT-PCR as described in the Supporting Information Section 1.1.

5.7.2. CYP2J2 inhibition in hiPSC-CMs

HiPSC-CMs were co-incubated with poyendarone, dronedarone or amiodarone (1 μmol/L) and CYP2J2 substrate, astemizole (1 μmol/L) in EB2 media for 24 h at 37 °C in a humidified atmosphere of 5% CO_2. The cells were then washed with 1× PBS twice and dislodged using Accutase® (Thermo Fisher Scientific) cell detachment solution. The cells were centrifuged, and the supernatant was discarded. The pellets were resuspended ice-cold ACN with 1 μmol/L buspirone (IS) and sonicated for 15 min on ice. The lysate was centrifuged and the supernatant was analyzed for the formation of *O*-desmethylastemizole using LC−MS/MS as described before[13]. The data was represented as percentage of CYP2J2 activity relative to control cells (no inhibitor).

5.7.3. Measurement of BTB variability in hiPSC-CMs

Electrophysiological perturbations of hiPSC-CMs were measured using multi-electrode array recording system (Multichannel Systems, Reutlingen, Germany). HiPSC-CMs were treated with dronedarone, poyendarone or amiodarone (0−10 μmol/L) and extracellular field potentials durations (FPD, equivalent to QTc) were measured for 5 min at baseline and 5 min after drug application as described before[71]. The local activation maps were generated using Cardio2D software (Multichannel Systems). FPD measurements were normalized (corrected FPD [cFPD]) to the beating rate of the contracting areas with the Bazzet correction formula: cFPD = FPD/((RR interval)^1/2) as described previously[72].

BTB variability in response to drug treatment was visualized in Poincare plots. Poincaré plots are a graphical representation where each point refers to the RR interval (beat cycle length) of n^{th}+1 cardiac beat that is being plotted against n^{th} beat. Poincaré plot descriptors SD1 (short term variability or STV_{RR}) and SD2 (long term variability or LTV_{RR}) define the extents of variability[73]. Poincaré plots with scattered points and incoherent alignment to the line to identity are indicative of BTB variability and *vice versa*. SD1 and SD2 changes due to dronedarone, poyendarone or amiodarone were measured at varying concentrations (0−10 μmol/L) using Kubios HRV2.2 (Department of Applied Physics, University of Eastern Finland, Kuopio, Finland)[74].

5.8. In vitro assessment of CYP2J2 knockdown on cardiac BTB variability

5.8.1. Cell culture

The human embryonic stem cells (ESCs) with a knocked in, constitutively expressed Genetically Encoded Calcium Indicator GCaMP6s were maintained on matrigel coated plates in StemMACS™ iPS-Brew XF (Miltenyi Biotec, Bergisch Gladbach, Germany) and passaged in clumps using Collagenase IV (1 mg/mL) enzymatic treatment. For differentiation, ESCs were passaged in single cells using Accutase (Nacalai Tesque, Kyoto, Japan), and subjected to the previously established small molecule based GiWi cardiomyocyte differentiation protocol[75]. On Day 7, the media was replaced with RPMI-1640 (GE Healthcare, Chicago, IL, USA) supplemented with B27 with insulin (B27+) (Miltenyi Biotec) for maturation and refreshed every 2 days. On Day 21, the glucose level in the media was slowly reduced to 0% by Day 28 to facilitate the metabolic selection of more matured cardiomyocytes that rely on β-oxidation. The cardiomyocytes (H7 CMs) were used for siRNA transfections on Day 28.

5.8.2. siRNA knockdown of CYP2J2

Set of four self-delivery modified Accell™ siRNAs (Table S1) and delivery media (Cat #B-005000, Dharmacon, Lafayette, CO, USA) were transfected into adherent cells following the supplier's protocol. Briefly, individual wells of Day 28 H7 CMs were treated with 1 μmol/L of an individual siRNA in Accell siRNA Delivery Media for 72 h. Control H7 CMs were treated with 1 μmol/L non-targeting siRNA. The delivery media was replaced with low glucose B27+ media for 24 h before video analysis and RNA harvesting for qPCR analysis to confirm CYP2J2 knockdown as described in Supporting Information Section 1.2.

5.8.3. Fluorescent Ca^{2+} imaging and video analysis of GCaMP6s H7 CMs

Calcium transients of H7 CM clusters post-treatment were imaged using a Nikon ECLIPSE Ti-S (Melville, NY, USA) fluorescent microscope and recorded using an Andor Zyla 4.2 sCMOS camera at 15 fps. Video data was analyzed using Nikon's NIS-Elements AR and processed using RStudio v1.2.1335 to identify fluorescent peaks corresponding to single cardiac contractions. Calcium transient durations were computed from the start of calcium depolarization to the 90% repolarization mark in each cardiac contraction, and the mean across all contractions was computed per cluster.

BTB intervals were computed as the time between two cardiac contractions. The interval mean and variation between beats were computed per cluster. Individual BTB intervals in each cluster were further utilized to generate Poincaré plots using the R library RHRV[76]. Each cardiac cluster generates a single Poincaré plot and two Poincaré parameters—SD1 (STV_{RR}) and SD2 (LTV_{RR}). The treatment groups were statistically compared using Poincaré parameters of the individual cardiac cluster as the dataset. To summarize the data for viewing purposes, the Poincaré plots were generated from combining data from all the clusters per treatment.

5.9. Measurement of anti-atrial fibrillatory properties and torsadogenic risk of poyendarone and dronedarone in persistent AF canine model

5.9.1. Animal husbandry

Experiments were performed on female beagle dogs (Kitayama Labes Co. Ltd., Nagano, Japan) weighing approximately 10 kg (n = 16). All experiments were reviewed and approved by Animal Care and User Committee of Toho University (No.19-52-396 and No.20-53-396), and performed according to the Guideline for the Care and Use of Laboratory Animals of Toho University, ARRIVE guidelines[77,78] and the NIH Guide for the Care and Use of Laboratory Animals.

5.9.2. Production of the chronic atrioventricular block dog and induction of persistent AF

After the animals (n = 16) were anesthetized with thiopental sodium (30 mg/kg, i.v.), catheter electrodes (Cordis-Webster Inc., CA, USA) were positioned at the compact atrioventricular node to develop the complete atrioventricular block with catheter ablation technique[41]. More than 1 month later, the dogs were initially anesthetized pentobarbital sodium (30 mg/kg, i.v.). After intubation, anesthesia was maintained by isoflurane inhalation (0.5%−1.5% *v/v*) vaporized in oxygen with a volume-limited ventilator. Tidal volume and respiratory rate were set at 20 mL/kg and 15

breaths/min, respectively. After a left fourth intercostal thoracotomy was performed, two sets of the electrode of temporary pacing lead (streamline atrial 6492; Medtronic Inc., MN, USA) were sutured onto the Bachmann bundle of the atria[50]. The pacing leads were connected to the rapid pulse-generating pacemaker (TNT-002AL; Taisho Biomed Instruments Co., Ltd., Osaka, Japan) placed at the gluteal region through the subcutaneous tunnel. More than 4 weeks after implanting the pacemaker, the atria were electrically driven at 400−600 bpm for >6 weeks. After confirming the onset of AF, the pacing was maintained at 600 bpm for another 2 weeks. Then, the atrial pacing was stopped under the monitoring of Holter electrocardiogram (QR2100; Fukuda M-E Kogyo Co., Ltd., Tokyo, Japan), and the duration of AF was assessed using the Holter analysis system (HS1000; Fukuda M-E Kogyo Co., Ltd.). If the AF persisted >24 h, the dog was judged for the use as the persistent AF model.

5.9.3. *Drug treatment*

Poyendarone hydrochloride was dissolved with 100% ethanol in a concentration of 20 mg/mL to prepare 3 mg/150 μL/kg. Dronedarone hydrochloride (Tokyo Chemical Industry Co., Ltd., Tokyo, Japan) and amiodarone hydrochloride were dissolved in the same manner. The other drugs used were thiopental sodium (Ravonal®, Mitsubishi-Tanabe Pharma Co., Osaka, Japan), pentobarbital sodium (Tokyo Chemical Industry Co., Ltd.), and isoflurane (isoflurane inhalation solution [Pfizer], Mylan Seiyaku Ltd., Osaka, Japan).

5.9.4. *Measurement of electrocardiogram*

The atria of the persistent AF model animal were electrically driven at 600 bpm for another 1 week. Under the monitoring of Holter electrocardiogram, the atrial pacing was stopped in conscious state. The 16 dogs were randomized into four groups to receive amiodarone, dronedarone, poyendarone or vehicle ethanol. As these dogs were prepared using highly consistent surgical procedures as described, there were no further specific blinding, inclusion and exclusion criteria. Approximately 2 h after the termination of the atrial pacing, poyendarone hydrochloride (3 mg/kg, $n = 4$), dronedarone hydrochloride (3 mg/kg, $n = 4$), amiodarone hydrochloride (3 mg/kg, $n = 4$) or vehicle ethanol (0.15 mL/kg, $n = 4$) was intravenously administered over 30 s. Then, the animals were caged and their Holter electrocardiogram was monitored for >21 h after the start of administration. These non-lethal doses of the drugs were based on previous experiments[40,79].

5.10. *Statistical analyses*

Statistical analyses were performed using GraphPad Prism software v8.4.2 (San Diego, CA, USA) unless otherwise mentioned. Values are presented as mean ± SEM or SD of experiments carried out at least twice with replicates. Statistical significance of differences between two groups was determined with Student's *t*-test, one-way or two-way analysis of variance (ANOVA) with Tukey's *post-hoc* test. The normality of data was determined by the Shapiro−Wilk test. Accordingly, nonparametric tests such as Mann−Whitney *U* (for two groups) or Kruskal−Wallis (for multiple groups) tests were used followed by Dunn's correction for multiple comparisons were used. Differences within parameters in *in vivo* studies were evaluated with one-way, repeated-measures ANOVA followed by contrasts as a post-hoc test for mean values comparison whereas those among the groups were done by one-way, factorial ANOVA followed by Tukey's multiple comparison testing. A P-value <0.05 was considered statistically significant.

Acknowledgments

This work was supported by the National University Heart Centre Singapore (NUHCS) Cardiovascular Research Institute (CVRI)−Core Fund [Grant NUHSRO/2019/082/Core], SCEPTRE CG Seed Grant [Grant NMRC/CG/M008/2017, Singapore], Singapore Ministry of Education Tier 1 Academic Research Funding [Grant R-148-000-193-112] and the National University of Singapore, Department of Pharmacy, Final Year Project Funding [Grant C-148-000-003-001] provided to Eric Chun Yong Chan and from Japan Society for the Promotion of Science (JSPS) KAKENHI [grant number 20K16136] provided to Ryuichi Kambayashi.

We sincerely thank Mr. Chen Yong Jun and Dr. Go Mei Lin from Drug Development Unit, Department of Pharmacy, National University of Singapore for performing the solubility and permeability studies. We acknowledge the contribution of Dr. Huang Hua from Electrophysiology Core and Dr. Soong Tuck Wah from Department of Physiology, Yong Loo Lin School of Medicine, National University of Singapore for performing the patch-clamp experiments. We are grateful to Dr. Thilo Hagen, Department of Biochemistry, Yong Loo Lin School of Medicine, National University of Singapore for providing access to Clarke-type oxygen electrode. We thank Dr. Ashish Mehta and Dr. Winston Shim, Research and Development Unit, National Heart Centre Singapore for their contribution to the *in vitro* multielectrode array experiments.

Author contributions

Participated in research design: Aneesh V. Karkhanis, Gopalakrishnan Venkatesan, Ryuichi Kambayashi, Eric Chun Yong Chan. Synthesized poyendarone: Gopalakrishnan Venkatesan. Performed *in vitro* experiments and analysed data: Aneesh V. Karkhanis, Jacqueline Wen Hui Leow, Marcus Qingrui Han, Hiroko Izumi-Nakaseko, Ai Goto, Jeremy Kah Sheng Pang, Boon Seng Soh. Performed *in vivo* animal experiments and analysed data: Ryuichi Kambayashi, Hiroko Izumi-Nakaseko, Ai Goto, Atsushi Sugiyama. Drafted the manuscript and contributed to manuscript review: Aneesh V. Karkhanis, Gopalakrishnan Venkatesan, Jacqueline Wen Hui Leow, Boon Seng Soh, Pipin Kojodjojo, Atsushi Sugiyama, Eric Chun Yong Chan.

Conflicts of interest

The authors have no conflicts of interest to declare.

Appendix A. Supporting information

Supporting data to this article can be found online at https://doi.org/10.1016/j.apsb.2022.03.008.

References

1. Roman RJ. P-450 metabolites of arachidonic acid in the control of cardiovascular function. *Physiol Rev* 2002;**82**:131−85.
2. DeLozier TC, Kissling GE, Coulter SJ, Dai D, Foley JF, Bradbury JA, et al. Detection of human CYP2C8, CYP2C9, and CYP2J2 in cardiovascular tissues. *Drug Metab Dispos* 2007;**35**:682−8.

3. Michaud V, Frappier M, Dumas MC, Turgeon J. Metabolic activity and mRNA levels of human cardiac CYP450s involved in drug metabolism. *PLoS One* 2010;**5**:e15666.
4. Wu S, Moomaw CR, Tomer KB, Falck JR, Zeldin DC. Molecular cloning and expression of CYP2J2, a human cytochrome P450 arachidonic acid epoxygenase highly expressed in heart. *J Biol Chem* 1996;**271**:3460−8.
5. Karkhanis A, Hong Y, Chan ECY. Inhibition and inactivation of human CYP2J2: implications in cardiac pathophysiology and opportunities in cancer therapy. *Biochem Pharmacol* 2017;**135**:12−21.
6. Zeldin DC, Moomaw CR, Jesse N, Tomer KB, Beetham J, Hammock BD, et al. Biochemical characterization of the human liver cytochrome P450 arachidonic acid epoxygenase pathway. *Arch Biochem Biophys* 1996;**330**:87−96.
7. Seubert J, Yang B, Bradbury JA, Graves J, Degraff LM, Gabel S, et al. Enhanced postischemic functional recovery in CYP2J2 transgenic hearts involves mitochondrial ATP-sensitive K+ channels and p42/p44 MAPK pathway. *Circ Res* 2004;**95**:506−14.
8. Zhang Y, El-Sikhry H, Chaudhary KR, Batchu SN, Shayeganpour A, Jukar TO, et al. Overexpression of CYP2J2 provides protection against doxorubicin-induced cardiotoxicity. *Am J Physiol Heart Circ Physiol* 2009;**297**:H37−46.
9. Wang X, Ni L, Yang L, Duan Q, Chen C, Edin ML, et al. CYP2J2-derived epoxyeicosatrienoic acids suppress endoplasmic reticulum stress in heart failure. *Mol Pharmacol* 2014;**85**:105−15.
10. Westphal C, Spallek B, Konkel A, Marko L, Qadri F, DeGraff LM, et al. CYP2J2 overexpression protects against arrhythmia susceptibility in cardiac hypertrophy. *PLoS One* 2013;**8**:e73490.
11. El-Sherbeni AA, El-Kadi AOS. Alterations in cytochrome P450-derived arachidonic acid metabolism during pressure overload-induced cardiac hypertrophy. *Biochem Pharmacol* 2014;**87**:456−66.
12. Althurwi HN, Maayah ZH, Elshenawy OH, El-Kadi AOS. Early changes in cytochrome P450s and their associated arachidonic acid metabolites play a crucial role in the initiation of cardiac hypertrophy induced by isoproterenol. *Drug Metab Dispos* 2015;**43**:1254−66.
13. Karkhanis A, Lam HY, Venkatesan G, Koh SK, Chai CLL, Zhou L, et al. Multiple modes of inhibition of human cytochrome P450 2J2 by dronedarone, amiodarone and their active metabolites. *Biochem Pharmacol* 2016;**107**:67−80.
14. Lee CA, Neul D, Clouser-Roche A, Dalvie D, Wester MR, Jiang Y, et al. Identification of novel substrates for human cytochrome P450 2J2. *Drug Metab Dispos* 2010;**38**:347−56.
15. Lee CA, Jones JP, Katayama J, Kaspera R, Jiang Y, Freiwald S, et al. Identifying a selective substrate and inhibitor pair for the evaluation of CYP2J2 activity. *Drug Metab Dispos* 2012;**40**:943−51.
16. Heijman J, Dobrev D. Pleiotropic actions of amiodarone: still puzzling after half a century. *Naunyn-Schmiedeberg's Arch Pharmacol* 2013;**386**:571−4.
17. Zipes DP, Prystowsky EN, Heger JJ. Amiodarone: electrophysiologic actions, pharmacokinetics and clinical effects. *J Am Coll Cardiol* 1984;**3**:1059−71.
18. Patel C, Yan GX, Kowey PR. Dronedarone. *Circulation* 2009;**120**:636−44.
19. Boriani G, Blomström-Lundqvist C, Hohnloser SH, Bergfeldt L, Botto GL, Capucci A, et al. Safety and efficacy of dronedarone from clinical trials to real-world evidence: implications for its use in atrial fibrillation. *EP Eur* 2019;**21**:1764−75.
20. Connolly SJ, Camm AJ, Halperin JL, Joyner C, Alings M, Amerena J, et al. Dronedarone in high-risk permanent atrial fibrillation. *N Engl J Med* 2011;**365**:2268−76.
21. Køber L, Torp-Pedersen C, McMurray JJV, Gøtzsche O, Lévy S, Crijns H, et al. Increased mortality after dronedarone therapy for severe heart failure. *N Engl J Med* 2008;**358**:2678−87.
22. Rosman J, Hoffmeister P, Reynolds M, Peralta A. Possible proarrhythmia with dronedarone. *J Cardiovasc Electrophysiol* 2013;**24**:103−4.
23. Huemer M, Sarganas G, Bronder E, Klimpel A, Garbe E, Haverkamp W. Torsade de pointes tachycardia in a patient on dronedarone therapy. *Pharmacother J Hum Pharmacol Drug Ther* 2015;**35**:e61−5.
24. Karkhanis A, Leow JWH, Hagen T, Chan ECY. Dronedarone-induced cardiac mitochondrial dysfunction and its mitigation by epoxyeicosatrienoic acids. *Toxicol Sci* 2018;**163**:79−91.
25. Karkhanis A, Tram NDT, Chan ECY. Effects of dronedarone, amiodarone and their active metabolites on sequential metabolism of arachidonic acid to epoxyeicosatrienoic and dihydroxyeicosatrienoic acids. *Biochem Pharmacol* 2017;**146**:188−98.
26. Luo YR. *Handbook of bond dissociation energies in organic compounds*. Boca Raton: CRC Press; 2002.
27. Wiberg KB. The Deuterium isotope effect. *Chem Rev* 1955;**55**:713−43.
28. Heijman J, Heusch G, Dobrev D. Pleiotropic effects of antiarrhythmic agents: dronedarone in the treatment of atrial fibrillation. *Clin Med Insights Cardiol* 2013;**7**:CMC.S8445.
29. Gant TG. Using deuterium in drug discovery: leaving the label in the drug. *J Med Chem* 2014;**57**:3595−611.
30. Chen C, Li G, Liao W, Wu J, Liu L, Ma D, et al. Selective inhibitors of CYP2J2 related to terfenadine exhibit strong activity against human cancers *in vitro* and *in vivo*. *J Pharmacol Exp Ther* 2009;**329**:908−18.
31. Lee E, Kim JH, Shon JC, Wu Z, Kim HJ, Gim M, et al. Terfenadone is a strong inhibitor of CYP2J2 present in the human liver and intestinal microsomes. *Drug Metab Pharmacokinet* 2018;**33**:159−63.
32. Leow JWH, Verma RK, Lim ABH, Fan H, Chan ECY. Atypical kinetics of cytochrome P450 2J2: epoxidation of arachidonic acid and reversible inhibition by xenobiotic inhibitors. *Eur J Pharm Sci* 2021;**164**:105889.
33. Liu KH, Kim MG, Lee DJ, Yoon YJ, Kim MJ, Shon JH, et al. Characterization of ebastine, hydroxyebastine, and carebastine metabolism by human liver microsomes and expressed cytochrome P450 enzymes: major roles for CYP2J2 and CYP3A. *Drug Metab Dispos* 2006;**34**:1793−7.
34. Evangelista EA, Kaspera R, Mokadam NA, Jones JP, Totah RA. Activity, inhibition, and induction of cytochrome P450 2J2 in adult human primary cardiomyocytes. *Drug Metab Dispos* 2013;**41**:2087−94.
35. Hong Y, Chia YMF, Yeo RH, Venkatesan G, Koh SK, Chai CLL, et al. Inactivation of human cytochrome P450 3A4 and 3A5 by dronedarone and *N*-desbutyl dronedarone. *Mol Pharmacol* 2016;**89**:1−13.
36. Mandel Y, Weissman A, Schick R, Barad L, Novak A, Meiry G, et al. Human embryonic and induced pluripotent stem cell-derived cardiomyocytes exhibit beat rate variability and power-law behavior. *Circulation* 2012;**125**:883−93.
37. Ben-Ari M, Schick R, Barad L, Novak A, Ben-Ari E, Lorber A, et al. From beat rate variability in induced pluripotent stem cell-derived pacemaker cells to heart rate variability in human subjects. *Heart Rhythm* 2014;**11**:1808−18.
38. Kambayashi R, Hagiwara-Nagasawa M, Kondo Y, Yeo ZJ, Goto A, Chiba K, et al. How the deuteration of dronedarone can modify its cardiovascular profile: *in vivo* characterization of electropharmacological effects of poyendarone, a deuterated analogue of dronedarone. *Cardiovasc Toxicol* 2020;**20**:339−50.
39. Motokawa Y, Nakamura Y, Hagiwara-Nagasawa M, Goto A, Chiba K, Lubna NJ, et al. *In vivo* analysis of the anti-atrial fibrillatory, proarrhythmic and cardiodepressive profiles of dronedarone as a guide for safety pharmacological evaluation of antiarrhythmic drugs. *Cardiovasc Toxicol* 2018;**18**:242−51.
40. Kambayashi R, Goto A, Nunoi Y, Hagiwara-Nagasawa M, Izumi-Nakaseko H, Venkatesan G, et al. An exploratory analysis of effects of poyendarone, a deuterated analogue of dronedarone, on the canine model of paroxysmal atrial fibrillation. *Naunyn-Schmiedeberg's Arch Pharmacol* 2021;**394**:1103−12.
41. Sugiyama A. Sensitive and reliable proarrhythmia *in vivo* animal models for predicting drug-induced torsades de pointes in patients with remodelled hearts. *Br J Pharmacol* 2008;**154**:1528−37.
42. Schofield J, Brasseur D, de Bruin B, Vassal T, Klieber S, Arabeyre C, et al. Effect of deuteration on the metabolism and clearance of some

pharmacologically active compounds—synthesis and *in vitro* metabolism of deuterated derivatives of dronedadrone. *J Label Compd Radiopharm* 2013;**56**:504−12.
43. Lu T, Hoshi T, Weintraub NL, Spector AA, Lee HC. Activation of ATP-sensitive K+ channels by epoxyeicosatrienoic acids in rat cardiac ventricular myocytes. *J Physiol* 2001;**537**:811−27.
44. Ke Q, Xiao YF, Bradbury JA, Graves JP, DeGraff LM, Seubert JM, et al. Electrophysiological properties of cardiomyocytes isolated from CYP2J2 transgenic mice. *Mol Pharmacol* 2007;**72**:1063−73.
45. Lu J, Chen A, Ma X, Shang X, Zhang Y, Guo Y, et al. Generation and characterization of cytochrome P450 2J3/10 CRISPR/Cas9 knockout rat model. *Drug Metab Dispos* 2020;**48**:1129−36.
46. Hueb W, Gersh BJ, Rezende PC, Garzillo CL, Lima EG, Vieira RD, et al. Hypotheses, rationale, design, and methods for prognostic evaluation of cardiac biomarker elevation after percutaneous and surgical revascularization in the absence of manifest myocardial infarction. A comparative analysis of biomarkers and cardiac magnetic resonance. The MASS-V Trial. *BMC Cardiovasc Disord* 2012;**12**:65.
47. Evangelista EA, Aliwarga T, Sotoodehnia N, Jensen PN, McKnight B, Lemaitre RN, et al. CYP2J2 modulates diverse transcriptional programs in adult human cardiomyocytes. *Sci Rep* 2020;**10**:5329.
48. Quayle JM, Nelson MT, Standen NB. ATP-sensitive and inwardly rectifying potassium channels in smooth muscle. *Physiol Rev* 1997;**77**:1165−232.
49. Loen V, Vos MA, van der Heyden MAG. The canine chronic atrioventricular block model in cardiovascular preclinical drug research. *Br J Pharmacol* 2022;**179**:859−81.
50. Kambayashi R, Izumi-Nakaseko H, Goto A, Tsurudome K, Ohshiro H, Izumi T, et al. Translational studies on anti-atrial fibrillatory action of oseltamivir by its *in vivo* and *in vitro* electropharmacological analyses. *Front Pharmacol* 2021;**12**:325.
51. Bossu A, Varkevisser R, Beekman HDM, Houtman MJC, van der Heyden MAG, Vos MA. Short-term variability of repolarization is superior to other repolarization parameters in the evaluation of diverse antiarrhythmic interventions in the chronic atrioventricular block dog. *J Cardiovasc Pharmacol* 2017;**69**:398−407.
52. Hinterseer M, Beckmann BM, Thomsen MB, Pfeufer A, Pozza RD, Loeff M, et al. Relation of increased short-term variability of QT interval to congenital long-QT syndrome. *Am J Cardiol* 2009;**103**:1244−8.
53. Thomsen MB, Verduyn SC, Stengl M, Beekman JDM, de Pater G, van Opstal J, et al. Increased short-term variability of repolarization predicts D-sotalol-induced torsades de pointes in dogs. *Circulation* 2004;**110**:2453−9.
54. Thomsen MB, Volders PGA, Beekman JDM, Matz J, Vos MA. Beat-to-beat variability of repolarization determines proarrhythmic outcome in dogs susceptible to drug-induced torsades de pointes. *J Am Coll Cardiol* 2006;**48**:1268−76.
55. Page RL, O'Bryant CL, Cheng D, Dow TJ, Ky B, Stein CM, et al. Drugs that may cause or exacerbate heart failure. *Circulation* 2016;**134**:e32−69.
56. Colatsky T, Fermini B, Gintant G, Pierson JB, Sager P, Sekino Y, et al. The comprehensive *in vitro* proarrhythmia assay (CiPA) initiative—update on progress. *J Pharmacol Toxicol Methods* 2016;**81**:15−20.
57. King LM, Ma J, Srettabunjong S, Graves J, Bradbury JA, Li L, et al. Cloning of CYP2J2 gene and identification of functional polymorphisms. *Mol Pharmacol* 2002;**61**:840−52.
58. Spiecker M, Darius H, Hankeln T, Soufi M, Sattler AM, Schaefer JR, et al. Risk of coronary artery disease associated with polymorphism of the cytochrome P450 epoxygenase CYP2J2. *Circulation* 2004;**110**:2132−6.
59. Liu PY, Li YH, Chao TH, Wu HL, Lin LJ, Tsai LM, et al. Synergistic effect of cytochrome P450 epoxygenase CYP2J2*7 polymorphism with smoking on the onset of premature myocardial infarction. *Atherosclerosis* 2007;**195**:199−206.
60. DeWitt SH, Maryanoff BE. Deuterated drug molecules: focus on FDA-approved deutetrabenazine. *Biochemistry* 2018;**57**:472−3.
61. Schmidt C. First deuterated drug approved. *Nat Biotechnol* 2017;**35**:493−4.
62. de Lera Ruiz M, Kraus RL. Voltage-gated sodium channels: structure, function, pharmacology, and clinical indications. *J Med Chem* 2015;**58**:7093−118.
63. Bartels P, Yu D, Huang H, Hu Z, Herzig S, Soong TW. Alternative splicing at N terminus and domain I modulates $Ca_V1.2$ inactivation and surface expression. *Biophys J* 2018;**114**:2095−106.
64. Liao P, Yu D, Li G, Yong TF, Soon JL, Chua YL, et al. A smooth muscle Cav1.2 calcium channel splice variant underlies hyperpolarized window current and enhanced state-dependent inhibition by nifedipine. *J Biol Chem* 2007;**282**:35133−42.
65. Vandenberg JI, Perry MD, Perrin MJ, Mann SA, Ke Y, Hill AP. hERG K^+ channels: structure, function, and clinical significance. *Physiol Rev* 2012;**92**:1393−478.
66. Cheong EJY, Goh JJN, Hong Y, Venkatesan G, Liu Y, Chiu GNC, et al. Application of static modeling—in the prediction of *in vivo* drug−drug interactions between rivaroxaban and antiarrhythmic agents based on *in vitro* inhibition studies. *Drug Metab Dispos* 2017;**45**:260−8.
67. Branco AF, Pereira SP, Gonzalez S, Gusev O, Rizvanov AA, Oliveira PJ. Gene expression profiling of H9c2 myoblast differentiation towards a cardiac-like phenotype. *PLoS One* 2015;**10**:e0129303.
68. Frezza C, Cipolat S, Scorrano L. Organelle isolation: functional mitochondria from mouse liver, muscle and cultured filroblasts. *Nat Protoc* 2007;**2**:287−95.
69. Lanza IR, Nair KS. Functional assessment of isolated mitochondria *in vitro*. *Methods Enzymol* 2009;**457**:349−72.
70. Mehta A, Chung YY, Ng A, Iskandar F, Atan S, Wei H, et al. Pharmacological response of human cardiomyocytes derived from virus-free induced pluripotent stem cells. *Cardiovasc Res* 2011;**91**:577−86.
71. Mehta A, Chung Y, Sequiera GL, Wong P, Liew R, Shim W. Pharmacoelectrophysiology of viral-free induced pluripotent stem cell-derived human cardiomyocytes. *Toxicol Sci* 2013;**131**:458−69.
72. Zwi L, Caspi O, Arbel G, Huber I, Gepstein A, Park IH, et al. Cardiomyocyte differentiation of human induced pluripotent stem cells. *Circulation* 2009;**120**:1513−23.
73. Jarosław P, Przemysław G. Filtering Poincaré plots. *CMST* 2005;**11**:39−48.
74. Tarvainen MP, Niskanen JP, Lipponen JA, Ranta-aho PO, Karjalainen PA. Kubios HRV-heart rate variability analysis software. *Comput Methods Programs Biomed* 2014;**113**:210−20.
75. Lian X, Zhang J, Azarin SM, Zhu K, Hazeltine LB, Bao X, et al. Directed cardiomyocyte differentiation from human pluripotent stem cells by modulating Wnt/β-catenin signaling under fully defined conditions. *Nat Protoc* 2013;**8**:162−75.
76. Martínez CAG, Quintana AO, Vila XA, Touriño MJL, Rodríguez-Liñares L, Presedo JMR, et al. *Heart rate variability analysis with the R package RHRV*. Springer International Publishing; 2017.
77. Kilkenny C, Browne W, Cuthill IC, Emerson M, Altman DG. Animal research: reporting *in vivo* experiments: the ARRIVE guidelines. *Br J Pharmacol* 2010;**160**:1577−9.
78. McGrath J, Drummond G, McLachlan E, Kilkenny C, Wainwright C. Guidelines for reporting experiments involving animals: the ARRIVE guidelines. *Br J Pharmacol* 2010;**160**:1573−6.
79. Matsukura S, Nakamura Y, Cao X, Wada T, Izumi-Nakaseko H, Ando K, et al. Anti-atrial fibrillatory *versus* proarrhythmic potentials of amiodarone: a new protocol for safety evaluation *in vivo*. *Cardiovasc Toxicol* 2017;**17**:157−62.
80. Spence S, Soper K, Hoe CM, Coleman J. The heart rate-corrected QT interval of conscious beagle dogs: a formula based on analysis of covariance. *Toxicol Sci* 1998;**45**:247−58.